



























## The CM carbonaceous chondrite regolith Diepenveen

Marco LANGBROEK <sup>1,2</sup>, Peter JENNISKENS <sup>2,3\*</sup>, Leo M. KRIEGSMAN <sup>1,4</sup>,  
Henk NIEUWENHUIS <sup>5</sup>, Niek DE KORT <sup>6</sup>, Jacob KUIPER <sup>7</sup>, Wim VAN WESTRENEN <sup>8</sup>,  
Michael E. ZOLENSKY <sup>9</sup>, Karen ZIEGLER <sup>10</sup>, Qing-Zhu YIN <sup>11</sup>, Matthew E. SANBORN <sup>11</sup>,  
Josh WIMPENNY <sup>11,12</sup>, Akane YAMAKAWA <sup>11,13</sup>, Sebastiaan J. DE VET <sup>1,6</sup>,  
Matthias M. M. MEIER <sup>14,15</sup>, Kees C. WELTEN <sup>16</sup>, Kunihiko NISHIZUMI <sup>16</sup>,  
Marc W. CAFFEE <sup>17</sup>, Aaron S. BURTON <sup>9,18</sup>, Jason P. DWORKIN <sup>18</sup>, Daniel P. GLAVIN <sup>18</sup>,  
Qinghao WU <sup>19</sup>, Richard N. ZARE <sup>19</sup>, Alexander RUF <sup>20</sup>, Mourad HARIR <sup>20</sup>, and  
Philippe SCHMITT-KOPPLIN <sup>20,21</sup>, The Diepenveen Meteorite Consortium

<sup>1</sup>Department of Research & Education, Naturalis Biodiversity Center, Darwinweg 2, 2333 CR, Leiden, the Netherlands

<sup>2</sup>Dutch Meteor Society, Leiden, the Netherlands

<sup>3</sup>SETI Institute, 189 Bernardo Ave, Mountain View, California 94043, USA

<sup>4</sup>Department of Earth Sciences, Utrecht University, Princetonlaan 8A, 3584 CB, Utrecht, the Netherlands

<sup>5</sup>Koninklijk Eise Eisinga Planetarium, Eisingastraat 3, 8801 KE, Franeker, the Netherlands

<sup>6</sup>Meteor Section, Royal Netherlands Association for Meteorology and Astronomy, Asmansweg 50, 2571 BK, Den Haag, the Netherlands

<sup>7</sup>Royal Netherlands Meteorological Institute, Utrechtseweg 297, 3731 GA, De Bilt, the Netherlands

<sup>8</sup>Department of Earth Sciences, Vrije Universiteit, De Boelelaan 1085, 1081 HV, Amsterdam, the Netherlands

<sup>9</sup>ARES, NASA Johnson Space Center, Mail Code X12, Houston, Texas 77058, USA

<sup>10</sup>Institute of Meteoritics, University of New Mexico, Albuquerque, New Mexico 87131, USA

<sup>11</sup>Department of Earth and Planetary Science, University of California Davis, One Shields Avenue, Davis, California 95616, USA

<sup>12</sup>Lawrence Livermore National Laboratory, 7000 East Ave, Livermore, California 94550, USA

<sup>13</sup>National Institute of Environmental Studies, 16-2 Onogawa, Tsukuba-City, Ibaraki 305-8506, Japan

<sup>14</sup>Naturmuseum St. Gallen, Rorschacherstrasse 263, CH-9016, St. Gallen, Switzerland

<sup>15</sup>Institute of Geochemistry and Petrology, ETH Zürich, CH-8092, Zürich, Switzerland

<sup>16</sup>Space Sciences Laboratory, University of California Berkeley, 7 Gauss Way, Berkeley, California 94720, USA

<sup>17</sup>Department of Earth, Atmospheric and Planetary Sciences and Department of Physics and Astronomy, Purdue University, West Lafayette, Indiana 47907, USA

<sup>18</sup>Solar System Exploration Division, NASA Goddard Space Flight Center, Greenbelt, Maryland 20771, USA

<sup>19</sup>Department of Chemistry, Stanford University, Zare Lab, Stanford, California 94305, USA

<sup>20</sup>Helmholtz Zentrum Munich, Ingolstaedter Landstrasse 1, D-86764 Neuherberg, Germany

<sup>21</sup>Technische Universität Muenchen, Maximus-von-Imhof-Forum 2, 85354 Freising, Germany

\*Corresponding author. E-mail: Petrus.M.Jenniskens@nasa.gov

(Received 24 December 2018; revision accepted 26 March 2019)

**Abstract**—A carbonaceous chondrite was recovered immediately after the fall near the village of Diepenveen in the Netherlands on October 27, 1873, but came to light only in 2012. Analysis of sodium and poly-aromatic hydrocarbon content suggests little contamination from handling. Diepenveen is a regolith breccia with an overall petrology consistent with a CM classification. Unlike most other CM chondrites, the bulk oxygen isotopes are extremely <sup>16</sup>O rich, apparently dominated by the signature of anhydrous minerals, distributed on a steep slope pointing to the domain of intrinsic CM water. A small subset plots closer to the normal CM regime, on a parallel line 2 ‰ lower in  $\delta^{17}\text{O}$ . Different lithologies in Diepenveen experienced varying levels of aqueous alteration processing, being less aqueously altered at places rather than more heated. The presence of an agglutinate

grain and the properties of methanol-soluble organic compounds point to active impact processing of some of the clasts. Diepenveen belongs to a CM clan with ~5 Ma CRE age, longer than most other CM chondrites, and has a relatively young K-Ar resetting age of ~1.5 Ga. As a CM chondrite, Diepenveen may be representative of samples soon to be returned from the surface of asteroid (162173) Ryugu by the Hayabusa2 spacecraft.

---

## INTRODUCTION

Diepenveen was recognized in the scientific community as a new CM (carbonaceous Mighei-like) chondrite only in 2012, after 139 years of obscurity in the *curiosa* collection of the former Rijks Hogere Burgerschool (Rijks HBS, Higher Civilian School) in Deventer, the Netherlands (Langbroek et al. 2015). It is a half 68.4 g individual with a break surface and approximately 50% fusion crust. A ~13 g fragment was glued back to the main fragment at an unknown date (Fig. 1A).

Unlike similar misplaced CM chondrites like Cochabamba (Kurat and Kracher 1975) and Paris (Hewins et al. 2014), Diepenveen has a known provenance. A hand-written card with the box in which it was stored (Fig. 1b) describes how the meteorite had fallen “with a blinding light and loud swishing sounds” on (Monday) October 27, 1873, near 3 P.M. local time, in an agricultural field near the village of Diepenveen (Fig. 2). Based on this note, the meteorite fell close to farm workers Albert Bos and his wife, who recovered it from a 45 cm deep pit in the sand within minutes after the fall, when it was still noticeably warm. Our genealogical research confirmed Bos and his wife to be inhabitants of Diepenveen, located at ~45 min walking distance from the farm where both were temporary laborers. Their link to the owner of the land, identified as Jan Willem IJsinck, was also verified. The farm still exists and is now a protected 18th century farm, pointing to a fall location within several hundred meters from 52.293°N, 6.125°E. Reportedly recovered from a sandy spot, the surrounding area of the farm is indeed characterized by sandy soil textures in present-day soil maps.

According to archival records that we recovered, Albert Bos lived a few houses down the road from village teacher Mr. te Wechel. The name of his stepson, Derk Herman te Wechel, is found at the bottom of the card that describes the circumstances of the fall and appears in the records of the Rijks HBS in Deventer (a town just a few miles from Diepenveen). The stepson was among the first students to graduate from the Rijks HBS and continued to study in Delft. After returning to Diepenveen and his subsequent marriage, he moved to Wageningen to work as a biologist, donating the

Diepenveen to his former Rijks HBS teachers some 5 years after the fall. After comparison of handwritings, it is likely that the small card was written by the Rijks HBS director Leendert A. J. Burgersdijk. Diepenveen survived two moves of the institute to other locations. In 1968, one of its last teachers was allowed to retrieve it from the schools *curiosa* collection just prior to when the school was closed and demolished.

Recovered within minutes after the fall, before rain could wet the meteorite (Fig. 2), Diepenveen is a CM chondrite fall new for study, like Sutter’s Mill (Jenniskens et al. 2012) and the recent Mukundpura meteorite (Ray and Shukla 2018), but with the possibility of some contamination from handling since 1873. CM chondrites are important as probes of the planetesimals that delivered water to the early Earth (Gounelle et al. 2005; Alexander et al. 2018) and is thought to be the type of material to be sampled in the ongoing Hayabusa2 mission to Cg-type asteroid (162173) Ryugu (Ishiguro et al. 2014; Perna et al. 2017; Kitazato et al. 2019), or even the OSIRIS-REx mission to B-type asteroid (101955) Bennu (Clark et al. 2011; Lauretta 2015; Lantz et al. 2018; Hamilton et al. 2019).

In this paper, we report on the petrology and mineralogy of Diepenveen, its isotopic signatures and cosmogenic nuclides, and investigate the level of contamination by terrestrial organic matter. We discovered that Diepenveen is a mostly uncontaminated regolithic breccia with properties unique to CM chondrites.

## SAMPLE AND EXPERIMENTAL METHODS

In January 2013, the stone was sampled at the Vrije Universiteit (VU) Amsterdam, the Netherlands. The preserved stone was dark and brittle. It crumbled easily. The fusion crust was thin (~1 mm) and looked fresh. The crust varied between black and an ochre tone with Munsell color 10YR 5/3 (Munsell 1954). This coloration might be indicative of soil remnants present in between asperities of the fusion crust. Diepenveen’s volume was determined using 3-D modeling of the stone using photogrammetry, implemented in the software Agisoft Photoscan Professional.

Figure 3 shows the areas that were sampled, which were well away from glue and fusion crust. Sampling was done in a porcelain dish clad in aluminum foil,

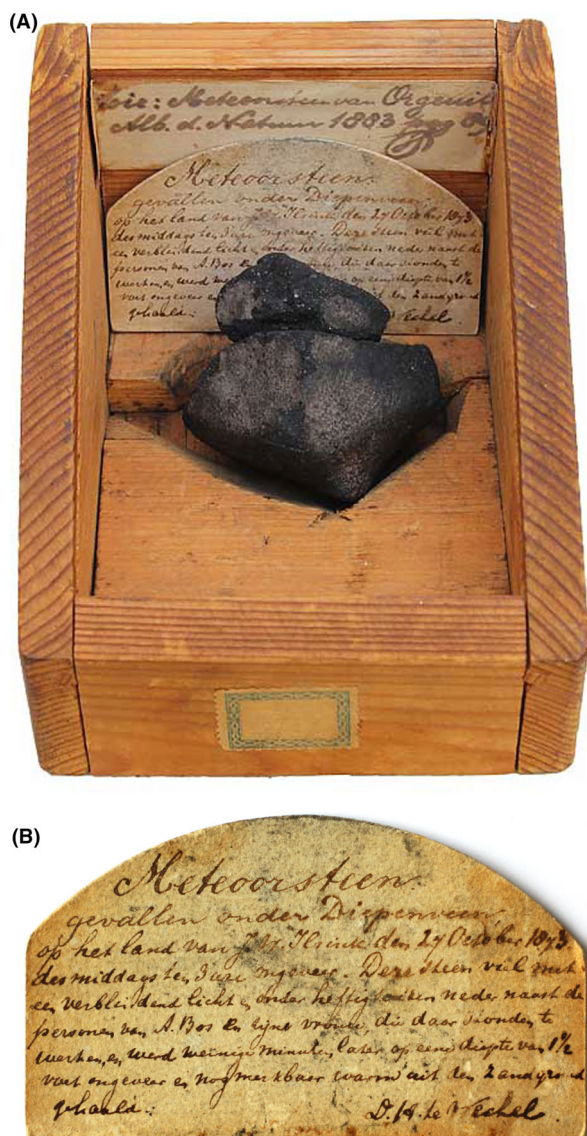


Fig. 1. A) Diepenveen meteorite as preserved since the fall in 1873. The box measures about 9.5 cm (width)  $\times$  11.5 cm (length), and its height varies from 3.3 cm (front) to 8.5 cm (back). B) Card kept with the meteorite. (Color figure can be viewed at [wileyonlinelibrary.com](http://wileyonlinelibrary.com).)

Note: The text reads: “Meteoorsteen gevallen onder Diepenveen, op het land van J.W. IJlsinck, den 27 October 1873, des middags te drie ongeveer. Deze steen viel met een verblindend licht, onder heftig suizen neder naast de personen van A. Bos en zijne vrouw, die daar stonden te werken, en werd weinig minuten later op een diepte van 1½ voet ongeveer en nog merkbaar warm uit den zandgrond gehaald. – D.H. te Wechel.” This translates to: “Meteor Stone fallen near Diepenveen on the land of J. W. IJlsinck on the 27th of October 1873 at approximately 3 o’clock in the afternoon. This stone fell with a blinding light and strong whistling sounds, close to the persons of A. Bos and his wife, who were working there, and was recovered from the sandy soil just few minutes later, from a depth of about 1.5 feet, and still noticeably warm. – D.H. te Wechel.”

using powder-free gloves and a metal razor blade. No fluids or additives were used during sampling. About 1.0 g of material was taken off, most as small fragments. Samples were stored in glass vials. The largest 0.58 g fragment was used to make two thick sections and a thin section for microprobe investigations.

Petrographic analysis by electron microprobe microanalyzer (EPMA) was done at Utrecht University, the Netherlands, at Naturalis in Leiden, and at NASA Johnson Space Center (JSC) to evaluate metamorphic conditions of the rock, to classify the meteorite, and to further explore shock metamorphic textures. At Utrecht, samples were analyzed with a JXA JEOL 8530F field emission EPMA at the Dutch National Geological Facility using natural mineral standards. In the early stages of the project, an older type of microprobe was used at the VU. In Leiden, a similar field emission gun scanning electron microscopy with energy dispersive X-ray spectroscopy (EDS) system was used for element mapping and spot analyses without standards, providing semiquantitative analyses for phase recognition.

At NASA JSC, the samples were imaged and analyzed using a JEOL 7600-FE scanning electron microscope, Cameca SX100 electron microprobe (EPMA), and JEOL 8530-FE electron microprobe at the E-beam laboratory of the Astromaterials and Exploration Science Division of JSC. Natural mineral standards were used. EPMA analyses at JSC were made at 15 kV and 20 nA. The moderately and highly shocked lithologies were analyzed separately, for comparison. The samples were also imaged using a JEOL 2000FX scanning transmission electron microscope with a Link EDS and image processing system.

At the University of California at Davis (UCD), the major, minor, and trace element abundances were determined in a homogenized powder of a 13.80 mg rock aliquot of Diepenveen using a Thermo Element XR high resolution inductively coupled plasma mass spectrometer (HR-ICP-MS) and methods described in Jenniskens et al. (2019) and Unsalan et al. (2019). A calibration curve for HR-ICP-MS was generated using a series of Allende Smithsonian reference powder solutions. In addition, a check standard of the CM chondrite Murchison was analyzed in the same analytical session. Both the Allende and Murchison standards were dissolved and diluted using the same procedures as the Diepenveen sample. The dilution factor for the major element aliquot analyzed was 39,687 $\times$  and 41,493 $\times$ , while trace elements were analyzed in an aliquot with a total dilution factor of 2525 $\times$  and 2495 $\times$ , for Diepenveen and Murchison, respectively. All dilutions were done by weight using a

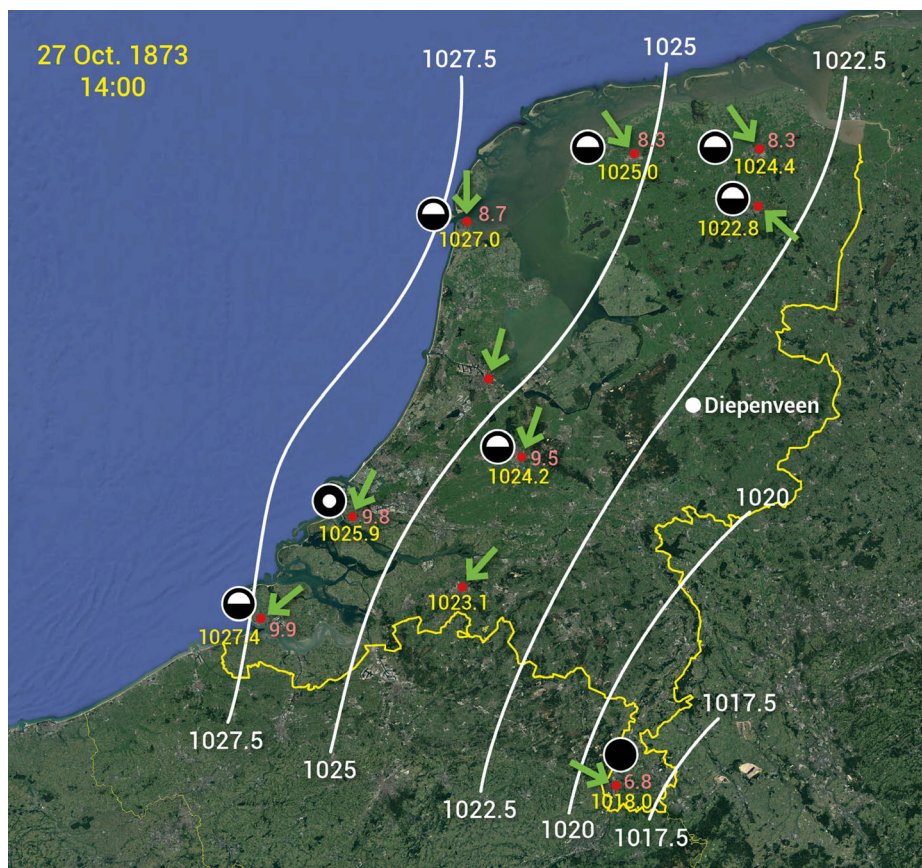


Fig. 2. Weather conditions over the Netherlands on October 27, 1873 at 2 P.M., the hour prior to the fall, on a Google Earth map of the present-day Netherlands. Symbols show the percentage of cloud cover, with numbers to their right showing the air temperature ( $^{\circ}\text{C}$ ) and below that the ground level pressure (hPa). White lines are pressure contours. The wind direction is shown by an arrow. (Color figure can be viewed at [wileyonlinelibrary.com](http://wileyonlinelibrary.com).)

five-digit Mettler Toledo balance. An internal spike composed of Re, In, and Bi was added to each vial for 10 ppb concentration to correct for instrumental drift that may occur during the analytical session, thus no data could be reported for these three elements.

The bulk composition of the major elements was measured also by averaging SEM-EDS (Leiden) and EPMA (Utrecht) transects in which up to 100 points are combined. Most transects measure  $1\text{ mm} \times 50\ \mu\text{m}$ .

At Naturalis, micro-XRF techniques were used to assess sample heterogeneity. Analyses were performed on rectangular domains of  $3 \times 2\text{ mm}$  on two polished thin sections (55 on one and 57 on the other) before carbon coating, using an EDAX Orbis micro-EDS desktop model analyzer. To characterize the matrix, several domains were selected in between chondrules and fragments, where the grain size was smaller than  $25\ \mu\text{m}$ . The micro-XRF signal for Na is on a large background shoulder for light elements and the data for Na were corrected by using a combination of EPMA and EDS data and estimates of mineral and matrix abundance.

Oxygen isotope studies were performed at the University of New Mexico using a dual inlet Thermo Finnigan MAT 253 mass spectrometer and methods described before (e.g., Popova et al. 2013; Jenniskens et al. 2019; Unsalan et al. 2019). Several aliquots of Diepenveen were measured against San Carlos olivine standards ( $\sim 1\text{--}2\text{ mg}$ ), which were analyzed daily. Each mass spectroscopic analysis consists of 20 cycles of standard-sample comparisons. Values are normalized to standard mean ocean water (SMOW). Excess  $\delta^{17}\text{O}'$  from the Terrestrial Fractionation Line  $\Delta^{17}\text{O}' = \delta^{17}\text{O}' - 0.528\ \delta^{18}\text{O}'$ , using a slope of 0.528 in the calculation (Barkan and Luz 2005), with the various notations described in, e.g., Jenniskens et al. (2019).

At UC Davis, ultrahigh-precision Cr isotope ratio measurements were completed in a powdered, bulk rock aliquot of Diepenveen using methods described before (e.g., Jenniskens et al. 2019; Unsalan et al. 2019). Chromium in a 10.43 mg powder aliquot was separated from the bulk rock matrix using a three-column cation and anion column chromatography procedure

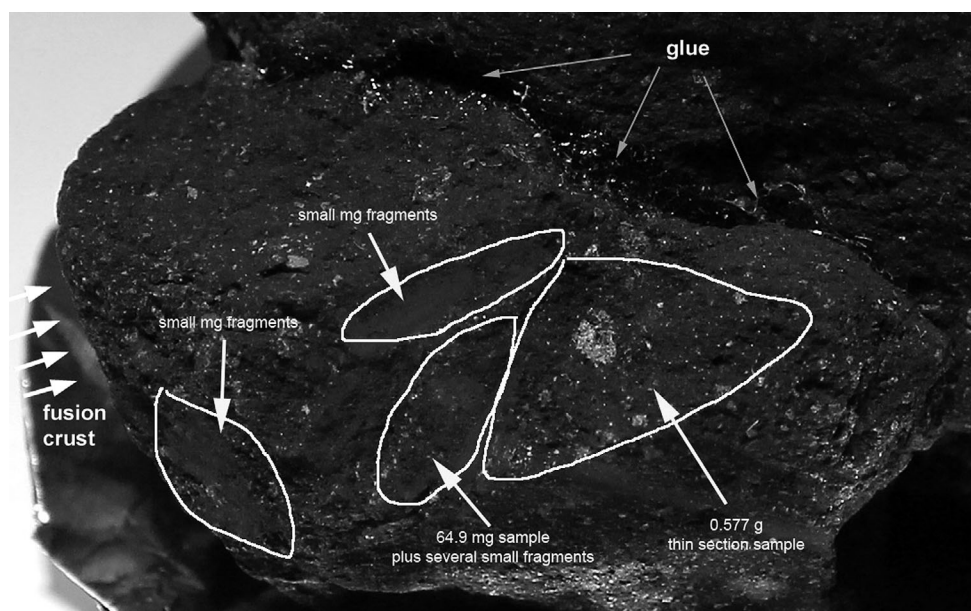


Fig. 3. Surface areas of Diepenveen sampled for this study. The broken surface is ~3.5 cm wide. Fragments extracted: D01 - 0.5773 g for two thin sections for petrography (VU and UNM); D02 - 64.9 mg; D03 - 62.5 mg for amino acids (NASA Goddard); D04 - 30.2 mg; D05 - 16.0 mg; D06 14.1 mg for PAHS (Stanford Univ.); D07 - 14.0 mg; D08 12.3 mg; D09 10.5 mg for oxygen isotopes (UNM); D10 - 9.7 mg. Bulk samples consisting of grit and dust/powder: D-A - 83.5 mg for bulk analysis (UCD); D-B - 37.2 mg for cosmogenic nuclides (UC Berkeley); D-C - 1.4 mg. VU = Vrije Universiteit; PAHS = polycyclic aromatic hydrocarbons; UCD = University of California at Davis.

previously described by Yamakawa et al. (2009). The isotopic composition of the Cr fraction was measured on the Thermo Triton Plus thermal ionization mass spectrometer at UC Davis. Mass fractionation was corrected for using an exponential law and a  $^{50}\text{Cr}/^{52}\text{Cr}$  ratio of 0.051859 (Shields et al. 1966).

At the Delft University of Technology, the meteorite's reflectance spectrum was determined using a PerkinElmer Lambda 1050S InGaAs spectrometer with an integrating sphere. The reflectance was calibrated against a  $\text{BaSO}_4$  white standard and the dark current was removed. A powdered, bulk rock aliquot of 0.1393 g was analyzed over the 0.35 to 2.45  $\mu\text{m}$  wavelength range in 1 nm increments ( $n = 3$  repetitions). Obtained data were averaged and normalized to unity at 0.55  $\mu\text{m}$ .

Noble gas measurements were performed with a custom-built noble gas mass spectrometer at ETH Zürich. Two samples of 20.7 and 43.0 mg each were prepared from a single, 64 mg fragment of Diepenveen. After weighing, the samples were wrapped in Al foil, loaded into the mass spectrometer, and then heated to 120 °C for 24 h to remove adsorbed atmospheric gases while exposed to ultrahigh vacuum. For noble gas extraction, the samples were heated to 1800 °C in a Mo crucible during a single temperature step and then analyzed using the protocol described in Wieler et al.

(1989). Blank contributions to sample runs were <0.1%, <2%, and <8% for all He, Ne, Ar isotopes, respectively.

For the analysis of the long-lived cosmogenic radionuclides  $^{10}\text{Be}$  (half-life =  $1.36 \times 10^6$  yr),  $^{26}\text{Al}$  ( $7.05 \times 10^5$  yr), and  $^{36}\text{Cl}$  ( $3.01 \times 10^5$  yr), 32.8 mg of Diepenveen was dissolved in an  $\text{HF}/\text{HNO}_3$  mixture along with ~0.94 mg of Be and 2.1 mg of Cl carriers. After isolation of Cl as  $\text{AgCl}$ , a small aliquot was taken for chemical analysis by inductively coupled plasma optical emission spectroscopy (ICP-OES). Be, Al, and Cl were separated and purified using procedures described previously (e.g., Nishiizumi 2004). Concentrations of  $^{10}\text{Be}$ ,  $^{26}\text{Al}$ , and  $^{36}\text{Cl}$  were measured by accelerator mass spectrometry (AMS) at Purdue University (Sharma et al. 2000). The measured  $^{10}\text{Be}/\text{Be}$ ,  $^{26}\text{Al}/\text{Al}$ , and  $^{36}\text{Cl}/\text{Cl}$  ratios are corrected for blank levels (which are <1% of the measured values) and normalized to AMS standards (Sharma et al. 1990; Nishiizumi 2004; Nishiizumi et al. 2007).

Several types of organic compounds were analyzed. At Stanford University, the organic fingerprint of polycyclic aromatic hydrocarbons (PAHs) was determined from a small aliquot from inside the meteorite (well away from glue), and from a fusion crust sample, both mounted on double-sided tape. The purpose was to determine the level of contamination from cigarette smoke and the like and to resolve, if

possible, an intrinsic PAH fingerprint. The sample was examined using two-step laser desorption laser ionization mass spectrometry (L<sup>2</sup>MS). This technology is able to ionize molecules with low ionization potentials. The method achieves minimal fragmentation owing to the controlled IR laser power in the desorption step and low photon energy in the ionization step (Wu et al. 2013). Doubly charged and multiple charged ions are not present in L<sup>2</sup>MS, and therefore they need not be considered. The background spectrum of the double-sided tape confirmed that this material does not give rise to contamination.

At the NASA Goddard Space Flight Center, amino acid measurements were made of a 63 mg fragment of Diepenveen using methods described previously (e.g., Jenniskens et al. 2012; Unsalan et al. 2019). In brief, the meteorite fragment was powdered in a ceramic mortar and pestle, 53.8 mg transferred to a borosilicate glass test tube, flame-sealed with 1 mL of Millipore Milli-Q Integral 10 (18.2 MΩ, < 1 ppb total organic carbon) ultrapure water and heated at 100 °C for 24 h. A procedural blank (glass tube with 1 mL Millipore water) was carried through the identical extraction protocol. After heating, one half of the water extract was transferred to a separate glass tube, dried under vacuum, and the residue subjected to a 6 M HCl acid vapor hydrolysis procedure at 150 °C for 3 h to determine total hydrolyzable amino acid content. The acid-hydrolyzed water extracts were desalted using cation-exchange resin (AG50W-X8, 100-200 mesh, hydrogen form, BIO-RAD), and the amino acids recovered by elution with 2 M NH<sub>4</sub>OH (prepared from Millipore water and NH<sub>3</sub>(g) (AirProducts, in vacuo). The remaining half of each water extract (nonhydrolyzed fraction) was taken through the identical desalting procedure in parallel with the acid-hydrolyzed extracts to determine the free amino acid abundances in the meteorites and soil sample. The amino acids in the NH<sub>4</sub>OH eluates were dried under vacuum to remove excess ammonia; the residues were then redissolved in 100 μL of Millipore water, transferred to sterile microcentrifuge tubes, and stored at -20 °C prior to analysis.

Based on analysis of amino acid standards taken through the entire extraction and acid hydrolysis procedure, no evidence was found of significant decomposition, racemization, or thermal degradation of the amino acids during the extraction procedure. The amino acids in the NH<sub>4</sub>OH eluates were derivatized with *o*-phthaldialdehyde/*N*-acetyl-L-cysteine (OPA/NAC) for 15 min at room temperature. The abundance, distribution, and enantiomeric compositions of the two- to six-carbon aliphatic amino acids present in the nonhydrolyzed and acid-hydrolyzed water extracts were

then determined by ultrahigh performance liquid chromatography fluorescence detection and time-of-flight mass spectrometry (hereafter LC-FD/ToF-MS) using a Waters ACQUITY H Class Ultra Performance Liquid Chromatography with fluorescence detector and Waters Xevo G2 XS. For the Xevo mass calibrations, an automatically applied lockmass of a fragment of Leucine Enkephalin (278.1141 Da) with a scan time of 1 s every 60 s is used. The capillary voltage was set to 1.2 kV. The amino acids and their enantiomeric ratios were quantified from the peak areas generated from both fluorescence detection and from the mass chromatogram of their OPA/NAC derivatives.

Methanol-soluble organic extracts for FT-ICR-MS analysis were prepared as described previously in Schmitt-Kopplin et al. (2010). Briefly, an intact fragment of about 20 mg weight was first washed with methanol (rapid contact with 1 mL methanol that was subsequently discarded) and immediately crushed in an agate mortar with 1 mL of LC/MS grade methanol and further transferred into an Eppendorf tube within an ultrasonic bath for 1 min. The tube was then centrifuged for 3 min. The supernatant methanol extract was directly used for infusion FT-ICR-MS. Before the sample extraction, great care was used to clean the agate pillar with solvent in an ultrasonic bath. A “blank” sample was produced by following the same extraction procedure without any meteorite fragment, and analyzed before and after the meteorite analysis. No significant mass peaks in the mass range of the meteorite extracts were observed. To fully exploit the advantages of Fourier transform ion cyclotron resonance mass spectrometry (FT-ICR-MS), instrument performance is routinely controlled by means of internal calibration on arginine clusters prior to any analysis. Relative *m/z* errors were usually <100 ppb across a range of 150 < *m/z* < 1500. The average mass resolution ranged near 1,000,000 at nominal mass 200, 400,000 at mass 400, and 300,000 at mass 600. Diepenveen methanol extracts were measured in negative electrospray ionization modes (ESI(-)) under conditions described earlier. About 3000 scans were accumulated with 4 Myr data points. The conversion of the exact masses into elementary composition is shown in more detail in Tziotis et al. (2011).

## RESULTS

### Petrography and Mineralogy

The petrography and mineralogy of Diepenveen is that of a CM chondrite (Zolensky et al. 1989, 1997). The meteorite is a polymict breccia with angular clasts

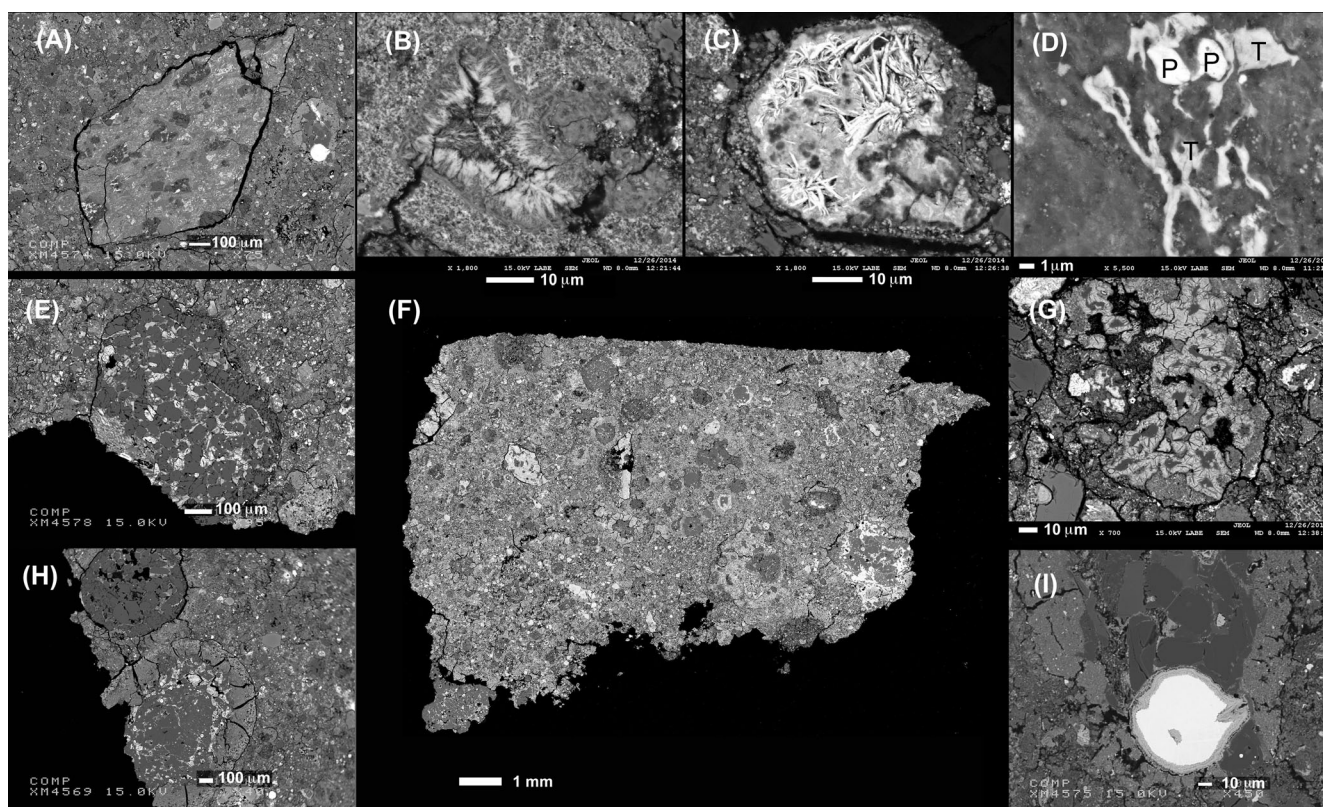


Fig. 4. Petrographic features of Diepenveen from SEM imaging. A) Unbrecciated CM2 clast. B) Phyllosilicate aggregate. C) Phyllosilicate aggregate, formed from alteration of a pyrrhotite crystal. D) Tochilinite crystals T next to Pyrrhotite P. E) Clast with amoeboid olivine aggregate. F) Mosaic of the Diepenveen thick section. G) CAI inclusion with spinel cores surrounded by phyllosilicate. H) Mildly altered low-FeO chondrule (top) with mantle grading into the matrix (top) next to a more altered low-FeO chondrule with poorly characterized phases clumps (light) and a thick rim with BSE-light top layer. I) Mantled low-FeO chondrule (olivine mantled by low-Ca pyroxene) with 70 micron Fe,Ni-metal inclusion (Fe/Ni = 15) with broad sulfide rim (Fe/Ni = 2). SEM = scanning electron microscopy; CAI = calcium-aluminum-rich inclusions.

of different CM lithologies measuring up to 1 mm in diameter (Figs. 4A–I). Brecciation is severe. Figure 4A, for example, shows a well-defined CM2 clast containing older clasts, indicating multiple impacts. The different CM lithologies vary with regard to hydration level of the matrix. The matrix is mainly fine-grained, and phyllosilicates are present locally. Figures 4B and 4C show phyllosilicate aggregates, with that in Fig. 4C formed from alteration of a pyrrhotite crystal. There is widespread tochilinite (Fig. 4D) and small clusters of phyllosilicates like Fig. 4B in some areas of matrix and in some of the clasts, which is common to most CMs (MacKinnon and Zolensky 1984; Pignatelli et al. 2017). There are no olivine pseudomorphs after phyllosilicates. One cluster of prismatic to acicular enstatite was found. Rare, tiny carbonate grains are present, which is usually typical only of more extensively altered CMs. Specific carbonates present are calcite, dolomite, and aragonite.

The matrix contains forsterite grains up to 0.4 mm (Langbroek et al. 2015), as well as amoeboid

olivine aggregates (Fig. 4E). Figure 4F shows the relative abundance of clasts, chondrules, and matrix. Pyroxenes show two types: low-Ca pyroxene (monoclinic state inferred from micro-Raman, using automated spectrum recognition based on the RRUFF database) and titanian-aluminian augite (“fassaite”). About 2–6 vol% of the matrix is metal and sulfides. FeNi grains measure up to 0.5 mm. All FeNi metal is kamacite with up to 2 wt% Cr and 1 wt% P. Olivine has a forsterite composition (Fo)  $35 \pm 10$  wt%, based on  $n = 5$  measurements (matrix); pyroxenes have ferrosillite composition (Fs):  $2 \pm 1$  (low-Ca pyroxene,  $n = 8$ ),  $1.8 \pm 0.2$  (fassaite,  $n = 5$ ) wt%; wollastonite (Wo):  $2 \pm 2$  (low-Ca pyroxene,  $n = 8$ ),  $44 \pm 4$  (fassaite,  $n = 5$ ) wt%. Some lithologies have more Fe-rich olivine: Fa 38–64 wt% (average Fa<sub>53</sub>,  $n = 9$ ), and their matrices contain significantly less phyllosilicates than the remainder of the meteorite. One 10 μm sized grain of nickel phosphide (Nazarov et al. 1996) was observed to be surrounded by matrix phyllosilicates.

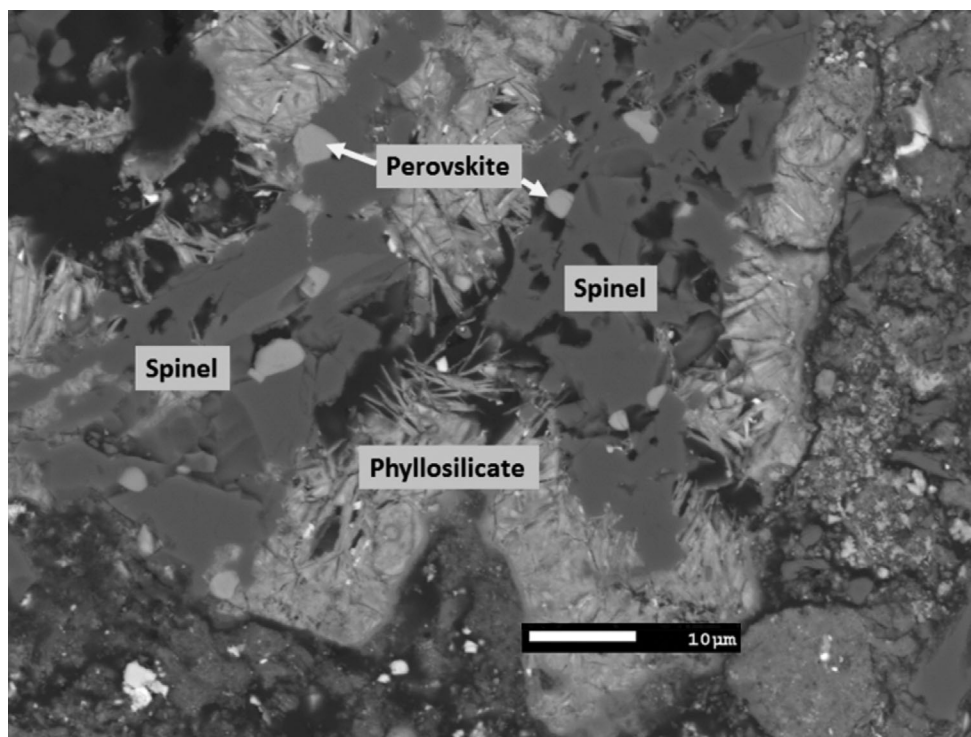


Fig. 5. Severely aqueously altered CAI. The diopside rim has been completely replaced by phyllosilicates rimming the surviving spinel grains, which contain scattered crystals of perovskite. CAI = calcium-aluminum-rich inclusions.

A total of 15–20 vol% of the mass consists of 0.05–0.7 mm sized chondrules (with a mean of 0.35 mm) (Langbroek et al. 2015), with one measured as large as 1.8 mm (Fig. 4H), similar to other CM meteorites (Brearley and Jones 1998; Trigo-Rodriguez et al. 2006). Many chondrules have thick fine-grained mantles. Most chondrules are porphyritic, only very few barred chondrules are present. Olivine has Fa:  $9 \pm 13$  (chondrules,  $n = 23$ ) and 70 (barred chondrule,  $n = 1$ ). Many chondrules are severely brecciated. One had a 70  $\mu\text{m}$  Fe,Ni-metal inclusion (Fig. 4I).

Calcium–aluminum-rich inclusions (CAI) are dominated by spinel crystals rimmed by diopside (Fig. 4G). The spinel crystals contain scattered perovskite grains (Fig. 5). Some of these CAI are highly altered by aqueous alteration, with rimming diopside replaced by phyllosilicates (Fig. 5). These features are typical of CAI in CM chondrites (MacPherson and Davis 1994). Two other CAIs have been mapped in detail. The first one is a fragment with blurred boundaries in the matrix. It consists of fassaite with small (2–3  $\mu\text{m}$ ), isolated perovskite inclusions. EPMA analyses also showed the presence of tiny Mg-spinel. Another CAI also shows perovskite and spinel inclusions. The second CAI is a similarly blurred patch within the largest observed fragment. It is completely dominated by fassaite and inclusions have not been

observed, but X-ray mapping highlight the Al- and Ti-rich core.

A small agglutinate grain was located in one thin section, consisting mainly of euhedral olivine crystals set in glass (Fig. 6), surrounded by porous, dehydrated phyllosilicates. Vesicles in the latter indicate loss of volume during phyllosilicate dehydration. This agglutinate grain is basically identical to those reported in other carbonaceous chondrites, and suggests a regolith setting for Diepenveen, with active impact processing (Zolensky et al. 2015; Lunning et al. 2016).

#### Density and Bulk Elemental and Mineral Composition

The volume of Diepenveen was measured at 32.34  $\text{cm}^3$ , giving a bulk density of  $2.12 \pm 0.03 \text{ g cm}^{-3}$ . This value is in line with the known densities range of  $2.12 \pm 0.26 \text{ g cm}^{-3}$  for CM chondrites (Britt and Consolmagno 2003).

The bulk major and trace element compositions of Diepenveen are summarized in Table 1, along with Murchison analyzed in the same analytical session at UCD and literature values of Murchison and Sutter's Mill for comparison (Jenniskens et al. 2012). Table 2 compares these data to independent results measured at UC Berkeley for cosmogenic nuclide studies,



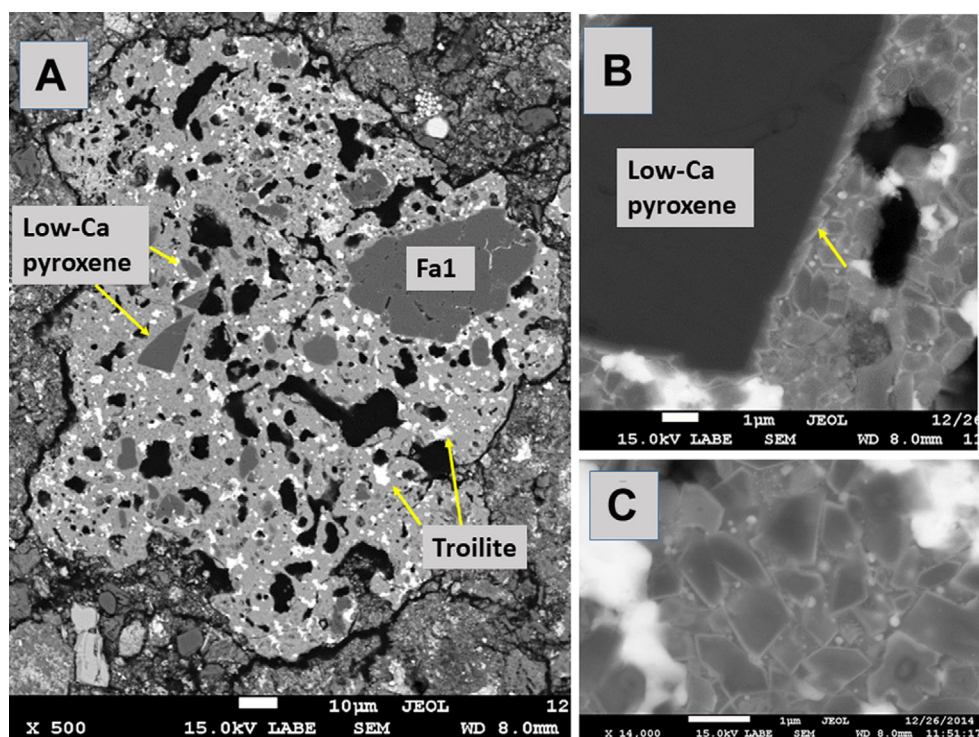


Fig. 6. A) Agglutinate grain in Diepenveen, a witness of regolith impact processing. Low-Ca pyroxene, olivine, and troilite are indicated. Vesicles are black. B) Close-up view of a low-Ca pyroxene crystal from (A), with an arrow indicating olivine crystals that have nucleated on its surface. C) Mesostasis of the agglutinate grain consists mainly of fine-grained, euhedral, normal-zoned olivine crystals in probable glass. (Color figure can be viewed at [wileyonlinelibrary.com](http://wileyonlinelibrary.com).)

which are in good agreement. UCD results are graphically displayed in Fig. 7. The bulk elemental composition of Diepenveen closely resembles that of other CM chondrites, such as Murchison and Sutter's Mill. They are distinctly different from those of CV chondrites.

Sodium and potassium are the most easily contaminated by handling of the meteorite over the years. Sodium is present at 0.39 wt% (Table 1), in between values for Murchison and Sutter's Mill SM51 (Jenniskens et al. 2012). Potassium is present at 580 ppm (Table 2). Probe data gave  $K = 210 \pm 170$ , with a broad spread between 0 and 1000 ppm in individual measurements (Table 2). Both are close to the elemental abundance of  $K = 400$  ppm in Wasson and Kallemeyn (1988). Both sodium and potassium abundances appear not significantly affected by handling.

EPMA line scans across matrix domains show moderate variation in the matrix bulk composition from place to place, mostly with low totals of accounted elements of ~80 wt%. Using the bulk composition from XRF and mineral compositions from EPMA as a basis, mass balance calculations show that the bulk composition equals ~33–34 vol% olivine, 2% low-Ca

pyroxene, 4% fassaite, 6% sulfide, 1% FeNi metal, and 53–54% hydrated matrix.

Carbon was not measured but typically accounts for only 2–4 wt% bulk in CM2 meteorites (Pearson et al. 2006). Water was not measured either. The water content in the bulk composition can be estimated on the assumption that tochilinite and serpentine (antigorite, lizardite) in the hydrated matrix are the only phases that were formed via a hydration reaction of olivine and sulfide. The bulk matrix can thus be recalculated as 43.5 vol% olivine (Fa26 on average), 28.6 vol% serpentine, 16.2 vol% tochilinite, 7.2 vol% fassaite, 1.2 vol% low-Ca Px, 3 vol% sulfide, and 0.3 vol% metal.

At an average 12–15 wt% water (hydroxyl) in the mineral structure, tochilinite and serpentine alone can explain about 6–7 wt% of water in the matrix. The best EPMA analyses of the Diepenveen matrix phyllosilicate compositions are shown in Fig. 8. Analyses were selected totaling between 74 and 95 wt%, which previous experience shows is the typical range for totals for serpentine and saponite in chondrites (Zolensky et al. 1993). All analyses with excessive S (>5 wt%) or P (>1 wt%) were eliminated. Sulfides were subtracted from the remaining analyses by removing sufficient Ni

Table 1. Bulk elemental composition by weight of Diepenveen (DV) and other CM chondrites Muchison (M) and Sutter's Mill 51 (SM).

		DV (this)	M (this)	M [1]	SM [2]
Li	ppm	1.33	1.22	1.40	1.66
Be	ppm	0.042	0.008	0.040	0.044
Na	wt%	0.390*	0.104	0.170	0.570
Mg	wt%	11.5	11.9	11.5	12.7
Al	wt%	1.10	1.24	1.13	1.27
Ca	wt%	1.23	1.04	1.29	1.41
Sc	ppm	8.63	8.84	8.18	9.23
Ti	ppm	644	642	650	700
V	ppm	67.4	66.5	68.0	77.2
Cr	ppm	2997	3008	3050	3100
Mn	ppm	1743	1876	1730	1800
Fe	wt%	20.7	21.1	21.3	22.4
Co	ppm	532	585	544	561
Cu	ppm	137	144	140	153
Zn	ppm	189	179	188	212
Ga	ppm	7.36	8.15	7.95	9.53
Rb	ppm	1.92	1.18	1.17	1.85
Sr	ppm	8.01	7.89	8.40	10.8
Y	ppm	2.29	2.28	2.35	2.42
Zr	ppm	7.05	5.65	6.90	7.90
Nb	ppm	0.390	0.416	0.440	0.494
Mo	ppm	2.84	1.59	1.80	1.11
Ru	ppm	1.56	1.20	1.40	0.886
Rh	ppm	0.107	0.111	0.130	0.170
Pd	ppm	0.700	0.843	0.752	0.860
Ag	ppm	0.115	0.119	0.125	0.150
Cd	ppm	0.421	0.401	0.398	-
Sn	ppm	0.761	0.802	0.890	1.35
Sb	ppm	0.158	0.181	0.140	0.120
Te	ppm	1.63	1.73	1.60	1.42
Cs	ppm	0.144	0.124	0.124	0.140
Ba	ppm	3.11	3.25	2.85	3.28
La	ppm	0.319	0.339	0.316	0.373
Ce	ppm	0.871	0.899	0.840	0.859
Pr	ppm	0.128	0.131	0.130	0.129
Nd	ppm	0.632	0.626	0.616	0.677
Sm	ppm	0.232	0.221	0.216	0.223
Eu	ppm	0.079	0.081	0.076	0.071
Gd	ppm	0.304	0.293	0.284	0.172
Tb	ppm	0.060	0.058	0.055	0.045
Dy	ppm	0.310	0.301	0.290	0.410
Ho	ppm	0.075	0.075	0.074	0.083
Er	ppm	0.220	0.222	0.216	0.230
Tm	ppm	0.039	0.037	0.037	0.041
Yb	ppm	0.225	0.218	0.211	0.249
Lu	ppm	0.040	0.041	0.039	0.040
Hf	ppm	0.168	0.158	0.161	0.143
W	ppm	0.110	0.142	0.150	0.129
Ir	ppm	0.597	0.589	0.607	0.650
Pt	ppm	1.08	1.05	0.990	1.30
Au	ppm	0.151	0.140	0.149	0.150
Tl	ppm	0.075	0.077	0.090	0.096
Pb	ppm	1.65	1.99	1.60	1.61
Th	ppm	0.044	0.051	0.043	0.047
U	ppm	0.011	0.009	0.010	0.013

\*Potentially contaminated by handling; [1] Friedrich *et al.* (2002); [2] Jenniskens *et al.* (2012).

Table 2. Bulk concentration (wt%) of major and minor elements measured by HR-ICP-MS (UCD), and ICP-OES (UC Berkeley) and electron microprobe (Naturalis). ICP-OES = inductively coupled plasma optical emission spectroscopy; UCD = University of California at Davis

Element	Diepenveen (UCD)	Diepenveen (UC Berkeley)	Diepenveen (Naturalis) <sup>1</sup>
Na	0.390	–	0.57 ± 0.06
Mg	11.5	11.6	8.3 ± 1.1
Al	1.10	1.10	1.02 ± 0.13
Si	–	–	11.3 ± 1.0
P	–	–	0.14 ± 0.10
S	–	–	2.37 ± 0.36
K	–	0.058	0.021 ± 0.017
Ca	1.23	1.31	0.58 ± 0.38
Ti	0.0644	–	0.040 ± 0.007
Cr	0.2997	–	0.31 ± 0.05
Mn	0.1743	0.16	0.17 ± 0.02
Fe	20.7	21.1	26.1 ± 2.6
Ni	–	1.11	1.64 ± 0.27
Co	0.0532	0.0530	(0.16)

<sup>1</sup>Average of 48 EPMA transects, Co based on Co/Ni ratio from micro-XRF.

and Fe to “use up” the S in the proportions (Fe + Ni)<sub>0.95</sub> S. The Si + Al-Mg-Fe atomic wt% ternary diagram of Fig. 8 also has added lines indicating the stoichiometric compositional ranges of typical serpentine and saponite.

Also shown (Fig. 8, right) is a similar diagram with many matrix phyllosilicate compositions from several CM chondrites from some of our recent, unpublished data collections at JSC. From Fig. 8 one can see that the phyllosilicates in Diepenveen plot at slightly higher Si + Al compositions than other CMs, probably indicating slightly more abundant admixture of saponite than is usually observed in CM chondrites matrix (Zolensky *et al.* 1993).

There are also matrix areas and clasts that have high-totalling analyses, indicating a lack of hydrous phases (Tonui *et al.* 2014). Very fine-grained sulfides are also more abundant than in typical CM matrix.

### Isotopic Compositions

Bulk oxygen isotope values measured at the University of New Mexico (Table 3) show unusually low  $\delta^{17}\text{O}'$  and  $\delta^{18}\text{O}'$  values ( $^{16}\text{O}$  rich), with more negative bulk values of  $\delta^{17}\text{O}'$  and  $\delta^{18}\text{O}'$  than typical for CM chondrites, some even lower than typical of CV, CO, and CK (Karoonda-like) meteorites (Fig. 9). The  $\delta^{17}\text{O}'$  values in one aliquot go as low as  $-13\%$ . They

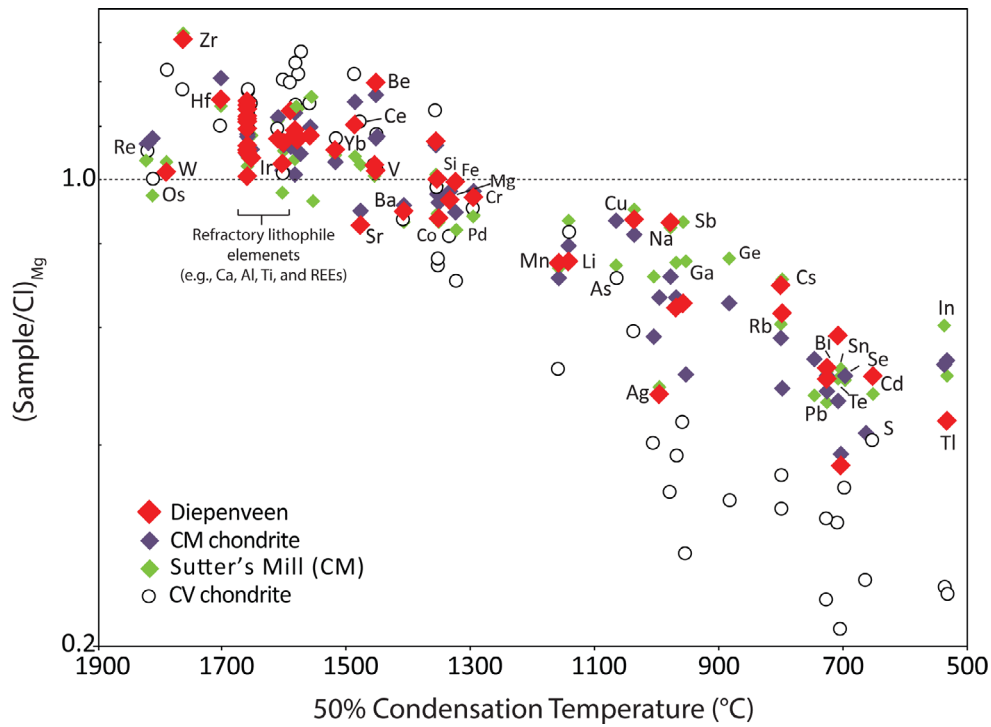


Fig. 7. Bulk elemental composition of Diepenveen normalized to Mg and CI chondrite versus the 50% condensation temperature of each element. Also shown for comparison are the elemental abundances average CV and CM chondrites, and Sutter's Mill (a CM chondrite). Data for the 50% condensation temperatures, CI, and CV chondrites abundances are from Lodders and Fegley (1998). Data for CM chondrites are from Lodders and Fegley (1998) and the Sutter's Mill meteorite are from Jenniskens et al. (2012). (Color figure can be viewed at [wileyonlinelibrary.com](http://wileyonlinelibrary.com).)

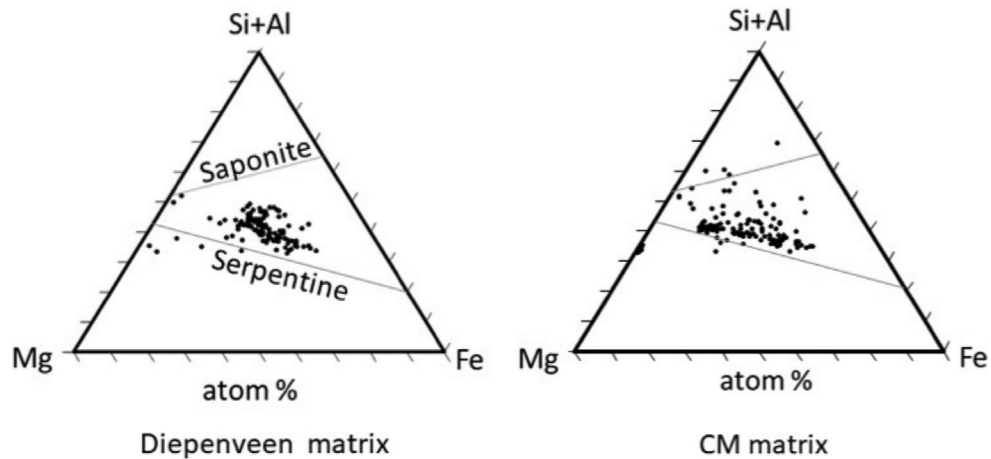


Fig. 8. Matrix phyllosilicate compositions in (left) Diepenveen (80 analyses) compared to (right) those in other CMs, including Boroskino (104 analyses), Crescent (39), MET01070 (75), Santa Cruz (27), and Cochabamba (81). Stoichiometric meteoritic compositional ranges for serpentine and saponite are indicated by the lines. Plotted compositions represent low-totaling (70–95 wt%) matrix analyses, with  $\text{SO}_3$  contents below 5 wt%, and for which the composition of pyrrhotite ( $[\text{Fe,Ni}]_{0.95}\text{S}$ ) has been subtracted.

are similar in  $\delta^{18}\text{O}' - \delta^{17}\text{O}'$  space to the anhydrous separates from Murchison (Clayton and Mayeda 1999) and acid-treated samples of Sutter's Mill (SM) SM2 and olivine grains of SM51 (Jenniskens et al. 2012, tables S10–S12).

The Cr isotopic compositions are shown as deviation of the  $^{53}\text{Cr}/^{52}\text{Cr}$  and  $^{54}\text{Cr}/^{52}\text{Cr}$  ratios from the terrestrial standard, presented in  $\epsilon$ -notation as parts per 10,000 deviation along with previously analyzed CM chondrites (Table 4). The Cr isotopic composition

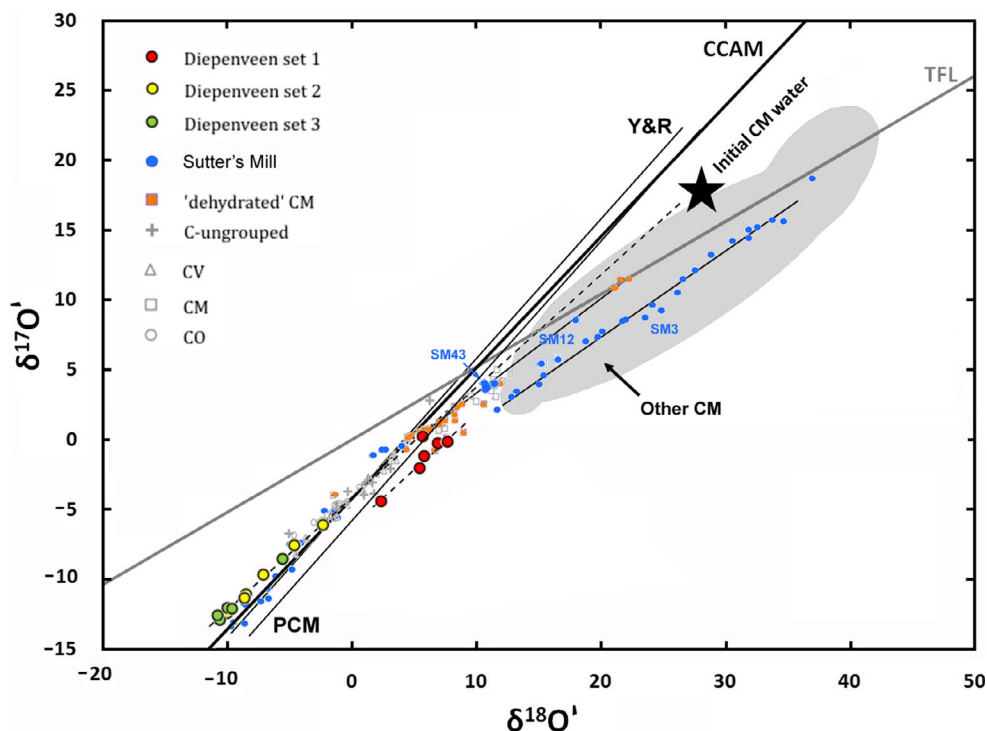


Fig. 9. Oxygen isotope values for Diepenveen in ‰ relative to SMOW, compared to other CM, CV, and CO type meteorites (Clayton and Mayeda 1999; Tonui et al. 2014), including Sutter's Mill (Jenniskens et al. 2012). The star marks the initial CM water proposed by Clayton and Mayeda (1999), with lines showing the Young and Russell (1998) slope of 1.00, the CCAM slope of 0.94 (Clayton and Mayeda 1999), the PCM (primitive chondrule minerals) line (Ushikubo et al. 2012), and the terrestrial fractionation line of slope 0.528 (Rumble et al. 2007). Other solid and dashed lines are discussed in the text. CCAM = carbonaceous chondrite anhydrous mineral. (Color figure can be viewed at [wileyonlinelibrary.com](http://wileyonlinelibrary.com).)

Table 3. Oxygen isotope values relative to ‰ V-SMOW for Diepenveen.

Sample via:	Set	Mass (mg)	Date	$\delta^{17}\text{O}'$	$\delta^{18}\text{O}'$	$\Delta^{17}\text{O}'$
UNM	1	1.2	Feb. 7, 2013	-0.243	6.946	-3.910
UNM	1	1.0	Feb. 7, 2013	-1.170	5.934	-4.303
UNM	1	1.1	Feb. 7, 2013	-4.305	2.501	-5.626
UNM	1	0.8	Feb. 7, 2013	-1.925	5.554	-4.858
UNM	1	1.3	Feb. 12, 2013	-0.044	7.689	-4.104
UNM	1	0.9	Feb. 12, 2013	0.301	5.771	-2.746
UCD	2	1.2	Oct. 20, 2014	-5.980	-2.114	-4.864
UCD	2	1.5	Oct. 20, 2014	-7.362	-4.343	-5.069
UCD	2	1.5	Oct. 20, 2014	-11.185	-8.273	-6.817
UCD	2	1.4	Dec. 2, 2014	-12.252	-9.590	-7.188
UCD	2	2.0	Dec. 2, 2014	-9.546	-6.795	-5.958
UCD	2	1.5	Dec. 2, 2014	-11.028	-8.147	-6.726
NL	3	2.3	Jan. 9, 2015	-8.406	-5.236	-5.641
NL	3	2.5	Jan. 9, 2015	-11.895	-9.220	-7.027
NL	3	2.7	Jan. 9, 2015	-11.884	-9.575	-6.828
NL	3	2.6	Jan. 9, 2015	-12.748	-10.137	-7.396
NL	3	2.8	Jan. 9, 2015	-12.417	-10.328	-6.964

$$\Delta^{17}\text{O}' = \delta^{17}\text{O}' - 0.528 \delta^{18}\text{O}'.$$

Table 4. Chromium isotope values for Diepenveen.

Sample	$\varepsilon^{53}\text{Cr}$	$\varepsilon^{54}\text{Cr}$
Diepenveen	$0.13 \pm 0.05$	$0.85 \pm 0.10$
Murchison (1)	$0.12 \pm 0.04$	$0.89 \pm 0.09$
Murchison (2)	$0.16 \pm 0.04$	$0.89 \pm 0.08$
Sutter's Mill SM43 (2)	$0.14 \pm 0.04$	$0.95 \pm 0.09$
Sutter's Mill SM51 (2)	$0.12 \pm 0.04$	$0.88 \pm 0.07$

Data from: (1) Yin et al. (2009); (2) Jenniskens et al. (2012).

measured in a bulk powder aliquot of Diepenveen at UC Davis yielded an  $\varepsilon^{54}\text{Cr}$  value of  $+0.85 \pm 0.10$ . This value is indistinguishable from the CM chondrites Murchison and Sutter's Mill (Jenniskens et al. 2012) and compares well to other CM (e.g., Göpel et al. 2015).

Figure 10 highlights the consistent  $\varepsilon^{54}\text{Cr}$  with typical CMs and variable nature of  $\Delta^{17}\text{O}'$  for Diepenveen. The overlap with Sutter's Mill in both isotopic compositions supports the conclusion that Diepenveen is a CM chondrite.

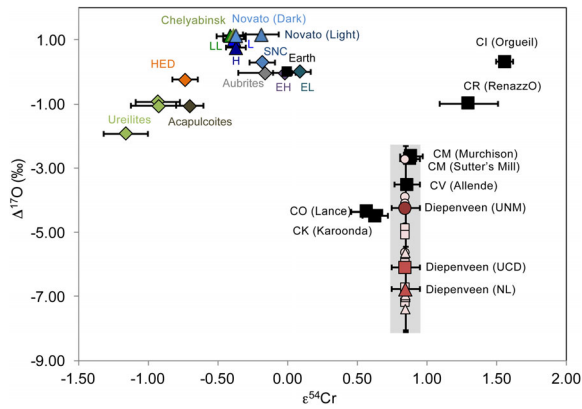


Fig. 10. The  $\epsilon^{54}\text{Cr}$  versus  $\Delta^{17}\text{O}$  systematics of Diepenveen in comparison to other achondrite and chondrite meteorite groups. Sources for the literature values are given in Jenniskens et al. (2014) and references therein. For Diepenveen, small data points represent individual  $\Delta^{17}\text{O}$  analyses for a given aliquot with different symbols (circle, square, and triangle) representing a different source for the material analyzed for oxygen isotopes. The larger symbols represent the average  $\Delta^{17}\text{O}$  for that aliquot. (Color figure can be viewed at [wileyonlinelibrary.com](http://wileyonlinelibrary.com).)

### Reflectance Spectrum

The reflectance spectrum of Diepenveen, normalized at  $0.55\ \mu\text{m}$ , is shown in Fig. 11. The

absolute reflectance (albedo) in the  $380\text{--}750\ \text{nm}$  range was  $0.123 \pm 0.015$ . The meteorite has a generally featureless visual spectrum with a positive slope toward the infrared. Weak spectral absorption bands in CM chondrites originate from olivine ( $0.85$ ,  $1.05$ , and  $1.25\ \mu\text{m}$ ), mixed valence Fe-bearing serpentine group phyllosilicates ( $0.70\text{--}0.75$ ,  $0.90\text{--}0.94$ ,  $1.07\text{--}1.13$ ,  $\sim 1.4$ , and  $2.32\ \mu\text{m}$ ), saponite group phyllosilicates ( $0.59\text{--}0.67$ ,  $0.89\text{--}0.90$ ,  $1.10\text{--}1.12$ ,  $\sim 1.4$ ,  $\sim 1.9$ ,  $\sim 2.3\ \mu\text{m}$ ), and magnetite ( $\sim 0.5$  and  $\sim 1.1\ \mu\text{m}$ ) (Cloutis et al. 2011). Diepenveen does not have the  $0.7\ \mu\text{m}$  absorption feature associated with the ferrous ( $\text{Fe}^{2+}$ ) to ferric ( $\text{Fe}^{3+}$ ) charge transfer common for oxidized iron in phyllosilicates (e.g., Vilas 2008), consistent with the general lack of well-formed phyllosilicates in the matrix. The band is lost also in thermal metamorphism due to the reduction of  $\text{Fe}^{3+}$  (e.g., Cloutis et al. 2012).

An effort to classify the spectrum following the Bus-DeMeo taxonomy (DeMeo et al. 2009) to relate Diepenveen to possible subtypes of the broad C-complex (C, Cg, Cgh, Ch, Cb, and B) did not reveal a unique solution (Fig. 11B). The drop-off short ward of  $0.5\ \mu\text{m}$  and the positive slope toward longer wavelengths exclude the Cb- and B-types, respectively. The overall featureless positive slope of Diepenveen's

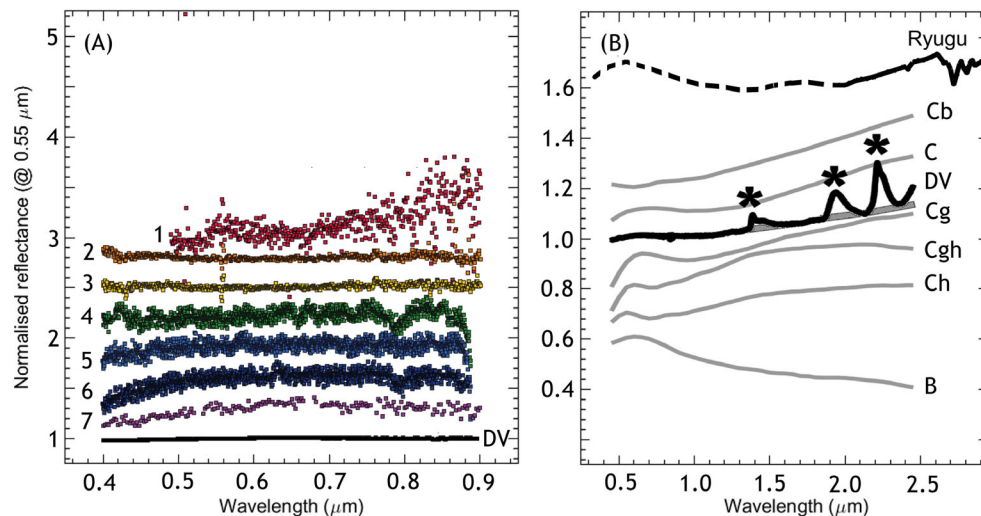


Fig. 11. Reflectance spectrum of Diepenveen (DV, dark line) (A) in the wavelength range of  $0.4\text{--}0.9\ \mu\text{m}$ . Results are compared to the spectrum of Cg-type asteroid (162173) Ryugu at different rotational phases from (#1–3) July 11, 2007, September 10, 2007, and September 11, 2007 (Vilas 2008); (#4–6) July 10, 2012, July 10, 2012, and July 9, 2012 (Lazzaro et al. 2013); and (#7) the 1999 apparition (Binzel et al. 2002). The spectra have been normalized to unity at  $0.55\ \mu\text{m}$  and are offset in steps of  $0.3$  for clarity (B) in the range  $0.45\text{--}2.45\ \mu\text{m}$  (before and after removal of water bands from absorbed telluric water in the  $\text{BaSO}_4$  standard, marked by an asterisk). Normalized results are compared to the spectra of C-class asteroids, offset in steps of  $\pm 0.1$  (DeMeo et al. 2009), and to the on-orbit (and ground-based, dashed) surface-averaged spectrum of Ryugu by Kitazato et al. (2019), offset by  $+0.7$ . (Color figure can be viewed at [wileyonlinelibrary.com](http://wileyonlinelibrary.com).)

spectrum most closely resembles that of the C and Cg asteroid spectral types.

### Cosmic Ray Exposure History

For the two Diepenveen samples measured, both two- and three-component mixtures yielded the same average concentration of cosmogenic  $^{21}\text{Ne}$ , of  $1.56 (\pm 0.19) \times 10^{-8} \text{ ccSTP g}^{-1}$  (Fig. 12). The cosmogenic  $^3\text{He}$  and  $^{21}\text{Ne}$  concentrations, however, differ by a factor of two between the two fragments (Table 5). Since the two fragments were only a few mm apart in the meteorite, this variation in cosmogenic noble gases cannot reflect different shielding conditions in space ( $4\pi$  exposure), but must reflect different exposure histories in a regolith, before compaction into a coherent rock that was later ejected as a meteoroid.

While the relationship between cosmogenic  $^{21}\text{Ne}$  and trapped  $^{20}\text{Ne}$  in some regolith breccias provides a good estimate of the cosmogenic  $^{21}\text{Ne}$  contribution produced during  $4\pi$  exposure (e.g., Wieler et al. 1989; Meier et al. 2014), this approach does not work for Diepenveen, as the intercept for this relationship at  $^{20}\text{Ne}_{\text{tr}} = 0$  is negative. In this respect, Diepenveen is probably more similar to Murchison, which shows two groups with similar trapped solar  $^{20}\text{Ne}$  contents but a difference of  $\sim 1 \times 10^{-8} \text{ cm}^3 \text{ g}^{-1}$  in cosmogenic

$^{21}\text{Ne}$  (Nakamura et al. 1999). In the case of Murchison, the cosmogenic  $^{21}\text{Ne}$  content of the low- $^{21}\text{Ne}$  group gives a good estimate of the  $4\pi$  exposure in space.

The relative contribution of cosmogenic Ne in most CM chondrites is too small to reveal the cosmogenic  $^{22}\text{Ne}/^{21}\text{Ne}$  ratio, which is often used to constrain the shielding conditions. Furthermore, cosmogenic  $^{21}\text{Ne}$  production rate can only be approximately estimated using noble gases alone. Given typical  $^{21}\text{Ne}$  production rates of  $0.15\text{--}0.30 \times 10^{-8} \text{ cm}^3 \text{ STP g}^{-1} \text{ Ma}$  in CM chondrites (e.g., Leya and Masarik 2009), the  $^{21}\text{Ne}$  concentration in Diepenveen #1 yields a CRE age in the range of 5–10 Ma, which includes regolith pre-irradiation. The  $4\pi$  CRE age must be lower, and is better constrained by Diepenveen #2, the sample with the lower  $^{21}\text{Ne}$  concentration, which yields an age range of 3–6 Ma. This age is a maximum  $4\pi$  age since a portion of cosmogenic  $^{21}\text{Ne}$  in Diepenveen #2 could be produced in regolith.

To get a better estimate of the  $^{21}\text{Ne}$  production rate, the measured cosmogenic  $^{26}\text{Al}$  concentration can be used as a shielding parameter (e.g., Graf et al. 1990). Using the model of Leya and Masarik (2009) for  $^{21}\text{Ne}$  and  $^{26}\text{Al}$  production rates in carbonaceous chondrites, the measured  $^{26}\text{Al}$  concentration in Diepenveen corresponds to a  $^{21}\text{Ne}$  production rate of  $0.16 (\pm 0.02) \times 10^{-8} \text{ cm}^3 \text{ STP g}^{-1} \text{ Ma}$

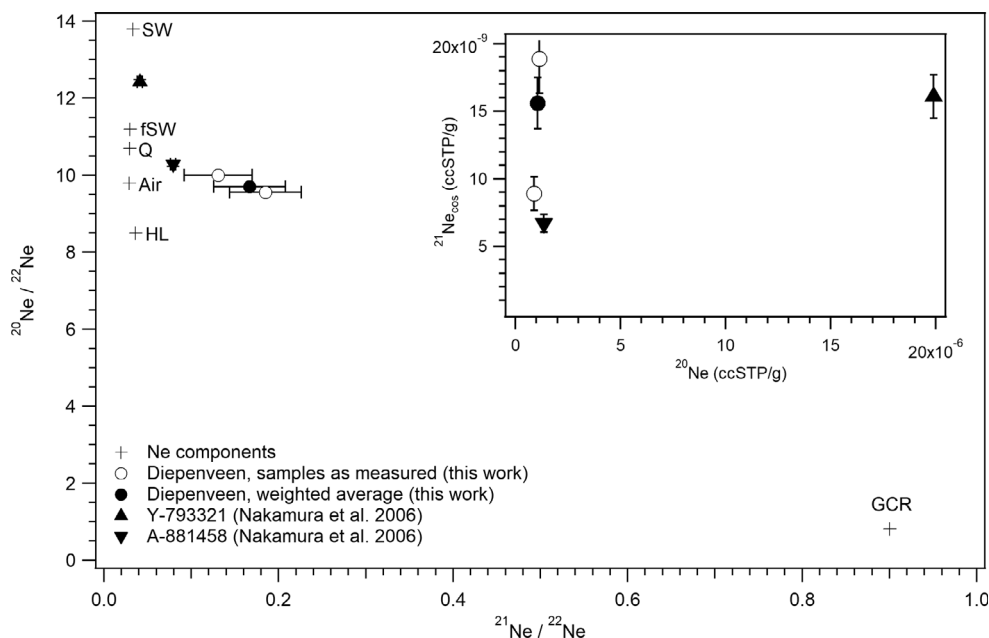


Fig. 12. Ne three-isotope plot (main) and  $^{21}\text{Ne}_{\text{cos}}$  versus  $^{20}\text{Ne}$  (inset). Noble gas components from Ott (2014). Crosses show the end member compositions of solar wind (SW), implantation mass-fractionated solar wind (fSW), primordial Q gases component found in “phase Q” (Q), Earth’s atmosphere (Air), primordial HL gases component enriched in both heavy and light elements found in presolar diamonds (HL), and galactic cosmogenic radionuclides (GCR).

Table 5. Noble gas concentrations for Diepenveen.

Sample	Diepenveen		Diepenveen		
	#1	#2	Total	Y-793321 (1)	A-881458 (1)
Mass (mg)	43.0	20.7	63.7	–	–
$^3\text{He}/^4\text{He}$	0.000595	0.000402	0.000533	0.000426	0.000380
$^4\text{He}_{\text{meas}}$	6660	5380	6250	82000	27000
$^{20}\text{Ne}/^{22}\text{Ne}$	9.556	9.998	9.699	12.43	10.29
$^{21}\text{Ne}/^{22}\text{Ne}$	0.185	0.131	0.167	0.041	0.079
$^{22}\text{Ne}_{\text{meas}}$	12.0	8.76	10.9	160	130
$^{36}\text{Ar}/^{38}\text{Ar}$	$5.3 \pm 0.4$	$4.8 \pm 2.4$	$5.1 \pm 1.1$	5.39	5.36
$^{40}\text{Ar}/^{36}\text{Ar}$	$8.9 \pm 0.8$	$11.5 \pm 1.0$	$9.5 \pm 1.0$	3.38	9.93
$^{36}\text{Ar}_{\text{meas}}$	n.d.	30.7	30.7	270	92
$^{21}\text{Ne}_{\text{cos}}$	1.89	0.891	1.56	1.61	0.671
P21	Typically $0.15\text{--}0.30 \text{ gMa}^{-1}$ for CM chondrites (2)				
T21 (Ma)	–	–	$\sim 5\text{--}10$	$\sim 5\text{--}11$	$\sim 2.2\text{--}4.5$
$^{40}\text{Ar}_{\text{rad}}^1$	n.d.	354	354	913	914
R40 (Ga)	–	–	1.5	2.6	2.6

All concentrations are given in units of  $10^{-8} \text{ cm}^3 \text{ STP g}^{-1}$  ( $= 4.46 \times 10^{-13} \text{ mol g}^{-1}$ ). Unless indicated otherwise, uncertainties are  $\sim 0.5\%$  for ratios and  $\sim 3\%$  for concentrations. (1) Nakamura (2006). (2) Leya and Masarik (2009).

<sup>1</sup>Assuming that all  $^{40}\text{Ar}$  is radiogenic.

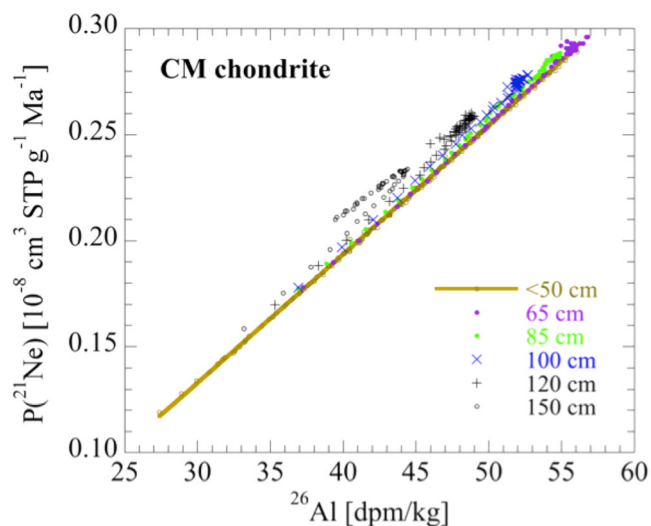


Fig. 13. Relationship between production rate of cosmogenic  $^{21}\text{Ne}$  and  $^{26}\text{Al}$  in CM chondrites with radii of 10–150 cm. The measured  $^{26}\text{Al}$  concentration of  $34.5 \pm 2.1 \text{ dpm/kg}$  corresponds to a  $^{21}\text{Ne}$  production rate of  $(0.16 \pm 0.02) \times 10^{-8} \text{ cm}^3 \text{ STP g}^{-1} \text{ Ma}^{-1}$ . (Color figure can be viewed at [wileyonlinelibrary.com](http://wileyonlinelibrary.com).)

(Fig. 13). This production rate yields an age of  $5.5 \pm 0.7 \text{ Ma}$  for Diepenveen-2. Again this age must be considered as an upper limit.

The concentrations of cosmogenic  $^{10}\text{Be}$  ( $17.2 \pm 0.1 \text{ dpm kg}^{-1}$ ),  $^{26}\text{Al}$  ( $34.5 \pm 2.1 \text{ dpm kg}^{-1}$ ) are slightly lower than average saturation values of 19–22 and 40–50  $\text{dpm kg}^{-1}$  in CM chondrites, respectively. The  $^{10}\text{Be}$  exposure age is 3–5 Ma. Assuming a CRE age of  $\sim 5 \text{ Ma}$  for Diepenveen, saturation values are

$\sim 19 \text{ dpm } ^{10}\text{Be kg}^{-1}$  and  $\sim 35 \text{ dpm } ^{26}\text{Al kg}^{-1}$ . Figure 14 shows that these are consistent with shielding condition in a smaller object (with radius,  $r = 10\text{--}20 \text{ cm}$ ) or near the surface of a much larger object ( $r \geq 1 \text{ m}$ ) (e.g., Masarik and Reedy 1994; Leya and Masarik 2009).

The concentration of cosmogenic  $^{36}\text{Cl}$  ( $10.5 \pm 2.1 \text{ dpm kg}^{-1}$ ) is slightly higher than the saturation value by spallation reactions on K, Ca, and Fe (the main target elements) alone, which is 6–7  $\text{dpm kg}^{-1}$ . The high  $^{36}\text{Cl}$  concentration indicates that Diepenveen contains an excess  $^{36}\text{Cl}$  component from thermal-neutron-captured reactions on  $^{35}\text{Cl}$ . The CM and CI chondrites contain higher hydrogen, H, concentration (1–2%) than other meteorites. The neutron spectrum and flux in meteorites are drastically changed by the H concentration (e.g., Lingenfelter et al. 1961). Although the H concentration in Diepenveen is not measured, the concentration is likely about 1–2% based on that of similar CM2 chondrites, Yamato-793321, and Asuka-881458 (Yanai et al. 1995). The excess of  $\sim 3 \text{ dpm } ^{36}\text{Cl kg}^{-1}$  meteorite corresponds to  $\sim 6\text{--}7 \text{ dpm } ^{36}\text{Cl g}^{-1} \text{ Cl}$ , assuming the Cl concentration in Diepenveen is 400–500 ppm, a typical value for CM chondrites (Ebihara and Sekimoto 2019). The 6–7  $\text{dpm g}^{-1} \text{ Cl}$  of neutron-captured  $^{36}\text{Cl}$  could be produced in a small CM chondrite with radius of  $r \sim 15 \text{ cm}$  (Kollár et al. 2006). In contrast, near the surface of a large CM, the production rates of thermal-neutron-captured  $^{36}\text{Cl}$  are too high compared to the measured value.

The  $^{21}\text{Ne}$  production rate of a radius 15–20 cm sized object is  $\sim 0.2 \times 10^{-8} \text{ cm}^3 \text{ STP g}^{-1} \text{ Ma}$  so that the maximum  $^{21}\text{Ne}$   $4\pi$ -exposure age is  $\sim 4.5 \text{ Ma}$ . In this

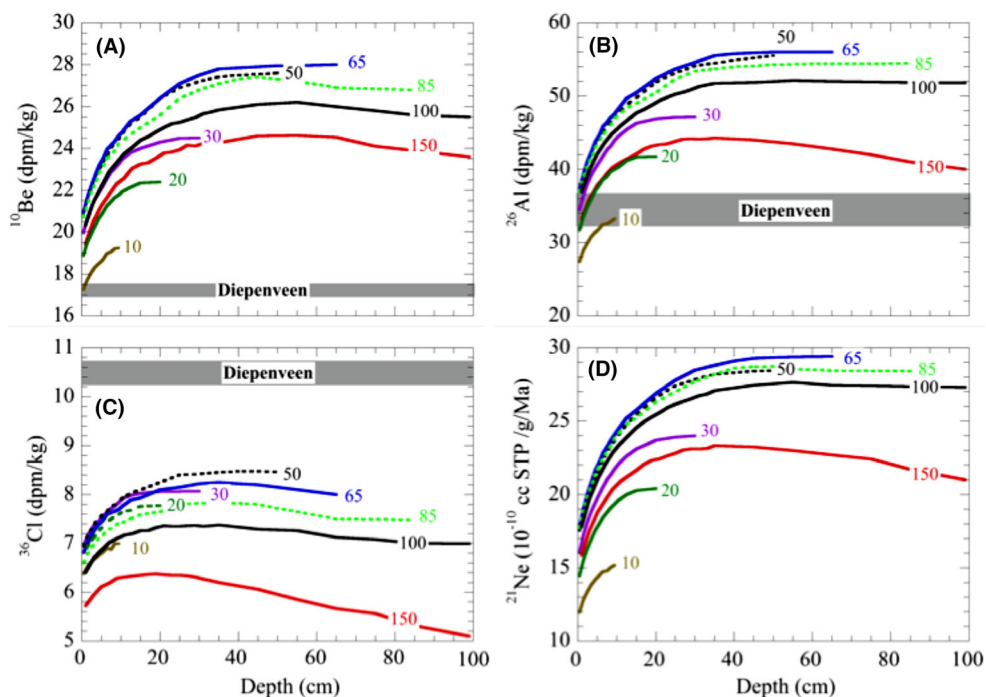


Fig. 14. Measured concentration of cosmogenic  $^{10}\text{Be}$  (A),  $^{26}\text{Al}$  (B), and  $^{36}\text{Cl}$  (C) in comparison with calculated production rates in CM chondrites with radii of 10–150 cm (Leya and Masarik 2009). Figure (D) shows production rates of  $^{21}\text{Ne}$  in CM chondrites with radii of 10–150 cm. (Color figure can be viewed at [wileyonlinelibrary.com](http://wileyonlinelibrary.com).)

scenario, the Diepenveen sample has a regolith CRE age of  $\sim 10$  Ma before compaction.

An alternative explanation would be a complex exposure history, in which part of the cosmogenic radionuclides and noble gases were produced in a larger object, followed by a recent breakup and delivery of a small fragment to Earth. However, if this breakup event occurred, it must have been very recent, since the  $^{26}\text{Al}/^{10}\text{Be}$  ratio of  $2.0 \pm 0.1$  is very close to calculated production rate ratios of 1.7–2.0 in CM chondrites of all sizes. Although the CRE history of Diepenveen is not fully constrained, a  $4\pi$  age of  $\sim 5$  Ma is consistent with both the cosmogenic radionuclide concentrations as well as the cosmogenic noble gas concentrations.

The measured  $^{40}\text{Ar}/^{36}\text{Ar}$  ratio is about 10, significantly lower than the atmospheric ratio of  $\sim 295$ , suggesting that the contribution of adsorbed air is minimal. Combining the  $^{40}\text{Ar}$  concentration measured in one fragment ( $3.54 \times 10^{-6} \text{ cm}^3 \text{ STP g}^{-1}$ ) with the average K concentration of 400 ppm for CM chondrites (Wasson and Kallemeyn 1988) results in a K-Ar retention age of  $\sim 1.49$  Ga. If the K concentration in the measured sample was 300 or 600 ppm, instead, then the K-Ar retention age are 1.80 or 1.11 Ga, respectively. Retention ages are valid if all gas was lost during the

gas-loss event. If some radiogenic Ar was retained, the gas-loss event is younger.

### Organic Composition

Common PAHs in cigarette smoke (Akin et al. 1976; Carré et al. 2005; Rodgman and Perfetti 2006; Wang et al. 2017) did not dominate the up to 30-C atom compounds detected in laser ionization mass spectrometry at Stanford University (Table 6). As expected, individual mass spectra show some intensity variations from one measurement to the next. The average spectra in Fig. 15 show that the PAH composition was similar to that of the ordinary L6 chondrite Novato (Jenniskens et al. 2014). The composition also compared well to that of Murchison (Gilmour and Pillinger 1992), which was remeasured in our laboratory (data not shown).

Although the ionization in  $\text{L}^2\text{MS}$  is very soft, strong peaks under 150 Da are observed, which is evidence for the existence of very fragile compounds, such as carboxylic acids and amino acids. It is likely that masses with  $m/z > 150$  Da are parent ions; elements of N are very likely to exist in ions over 150 Da deduced from the appearance of odd molecular weights. The fragment at  $m/z = 26$  indicates



Table 6. Mass peak assignments for PAH compounds detected in Diepenveen (DV) and for compounds found in cigarette smoke measured by UV photo-ionization and time-of-flight mass spectroscopy (Wang et al. 2017). PAH = polycyclic aromatic hydrocarbon.

$m/z$	Assignments	Diepenveen (CM, bulk)	Diepenveen (CM, crust)	Novato (L6)	Cigarette smoke
23	Na <sup>+</sup>	x	x	x	n.d. <sup>1</sup>
24	Mg <sup>+</sup>	x	x	x	n.d.
25	C <sub>2</sub> H <sup>+</sup>	x	x	x	n.d.
26	CN <sup>+</sup>	x	x	x	n.d.
27	HCN <sup>+</sup> /C <sub>2</sub> H <sub>3</sub> <sup>+</sup>	–	–	–	x
28	CO <sup>+</sup>	x	x	–	x
30	NO <sup>+</sup> , C <sub>2</sub> H <sub>2</sub> O <sup>+</sup>	–	–	–	x
39	K <sup>+</sup> /C <sub>3</sub> H <sub>3</sub> <sup>+</sup>	–	–	x	–
42	CH <sub>3</sub> CHCH <sub>2</sub> <sup>+</sup>	–	–	–	x
43	CH <sub>3</sub> CO <sup>+</sup> /CH <sub>2</sub> CNH <sub>2</sub> <sup>+</sup> /C <sub>3</sub> H <sub>7</sub> <sup>+</sup>	x	x	x	x
44	C <sub>2</sub> H <sub>4</sub> O <sup>+</sup>	–	–	–	x
48	Ti <sup>+</sup> /CH <sub>3</sub> SH <sup>+</sup> /SO <sup>+</sup>	x	x	–	x
54	C <sub>4</sub> H <sub>6</sub> <sup>+</sup>	–	–	–	x
55	C <sub>4</sub> H <sub>7</sub> <sup>+</sup> /CH <sub>3</sub> CH <sub>2</sub> CN <sup>+</sup>	x	x	x	–
56	C <sub>4</sub> H <sub>8</sub> <sup>+</sup> /C <sub>3</sub> H <sub>4</sub> O <sup>+</sup> /Fe <sup>+</sup>	x	x	x	x
57	C <sub>2</sub> H <sub>5</sub> CO <sup>+</sup> /C <sub>4</sub> H <sub>9</sub> <sup>+</sup> /C <sub>3</sub> H <sub>7</sub> N <sup>+</sup>	x	x	x	–
58	CH <sub>3</sub> CH <sub>2</sub> CHO <sup>+</sup> /C <sub>2</sub> H <sub>5</sub> CHNH <sub>2</sub> <sup>+</sup> /C <sub>4</sub> H <sub>10</sub> <sup>+</sup>	x	x	x	x
59	C <sub>3</sub> H <sub>7</sub> O <sup>+</sup> /CH <sub>3</sub> CH <sub>2</sub> CH <sub>2</sub> NH <sub>2</sub> <sup>+</sup> /C <sub>2</sub> H <sub>7</sub> N <sub>2</sub> <sup>+</sup>	–	–	–	–
64	S <sub>2</sub> <sup>+</sup> /Zn <sup>+</sup> /C <sub>3</sub> N <sub>2</sub> <sup>+</sup>	x	x	–	–
67	C <sub>5</sub> H <sub>7</sub> <sup>+</sup> /C <sub>4</sub> H <sub>5</sub> N <sup>+</sup> /C <sub>4</sub> H <sub>3</sub> O <sup>+</sup>	–	–	x	–
68	C <sub>5</sub> H <sub>8</sub> <sup>+</sup>	–	–	–	x
69	C <sub>5</sub> H <sub>9</sub> <sup>+</sup> /C <sub>4</sub> H <sub>7</sub> N <sup>+</sup> /C <sub>4</sub> H <sub>5</sub> O <sup>+</sup>	x	x	x	–
70	C <sub>4</sub> H <sub>6</sub> O <sup>+</sup>	–	–	–	x
71	C <sub>4</sub> H <sub>9</sub> N <sup>+</sup> /C <sub>4</sub> H <sub>7</sub> O <sup>+</sup> /C <sub>3</sub> H <sub>7</sub> N <sub>2</sub> <sup>+</sup>	x	x	x	x
72	C <sub>4</sub> H <sub>8</sub> O <sup>+</sup>	–	–	–	x
78	C <sub>6</sub> H <sub>6</sub> <sup>+</sup>	–	–	–	x
79	C <sub>5</sub> H <sub>5</sub> N <sup>+</sup>	–	–	–	x
81	C <sub>5</sub> H <sub>7</sub> N <sup>+</sup> /C <sub>6</sub> H <sub>9</sub> <sup>+</sup>	x	x	x	–
82	C <sub>6</sub> H <sub>10</sub> <sup>+</sup>	–	–	–	x
83	C <sub>5</sub> H <sub>9</sub> N <sup>+</sup> /C <sub>6</sub> H <sub>11</sub> <sup>+</sup>	–	x	x	–
85	C <sub>5</sub> H <sub>11</sub> N <sup>+</sup> /C <sub>6</sub> H <sub>13</sub> <sup>+</sup> /C <sub>5</sub> H <sub>9</sub> O <sup>+</sup>	x	x	x	–
86	C <sub>6</sub> H <sub>14</sub> <sup>+</sup>	–	–	–	x
91	C <sub>7</sub> H <sub>7</sub> <sup>+</sup> /C <sub>6</sub> H <sub>5</sub> N <sup>+</sup>	x	x	x	–
92	C <sub>7</sub> H <sub>8</sub> <sup>+</sup>	–	–	–	x
94	C <sub>6</sub> H <sub>5</sub> OH <sup>+</sup>	–	–	–	x
96	–	–	–	–	x
97	C <sub>6</sub> H <sub>11</sub> N <sup>+</sup> /C <sub>5</sub> H <sub>5</sub> O <sub>2</sub> <sup>+</sup>	x	x	x	–
106	–	–	–	–	x
107	C <sub>7</sub> H <sub>9</sub> N <sup>+</sup>	x	x	x	–
113	C <sub>7</sub> H <sub>15</sub> N <sup>+</sup>	–	–	x	n.d.
134	C <sub>10</sub> H <sub>14</sub> <sup>+</sup> /C <sub>9</sub> H <sub>10</sub> O <sup>+</sup>	x	x	–	n.d.
206	C <sub>16</sub> H <sub>14</sub> <sup>+</sup>	–	–	x	n.d.
207	C <sub>15</sub> H <sub>13</sub> N <sup>+</sup> /C <sub>12</sub> H <sub>21</sub> N <sub>3</sub> <sup>+</sup>	–	–	x	n.d.
208	C <sub>16</sub> H <sub>16</sub> <sup>+</sup> /C <sub>15</sub> H <sub>12</sub> O <sup>+</sup>	–	–	x	n.d.

<sup>1</sup>n.d. = no data.

the existence of -CN groups in the Diepenveen meteorite. The  $m/z = 28$  and 45 are evidence for -COOH groups.

Measurements on the amino acids obtained at the NASA Goddard Space Flight Center show that for the

chiral proteinogenic amino acids (e.g., aspartic acid, glutamic acid, serine, threonine, alanine, and valine), the L-enantiomers are present in higher abundance (D/L ratios ranging from ~ 0.01 to 0.35), indicating that some terrestrial contamination after the fall has occurred

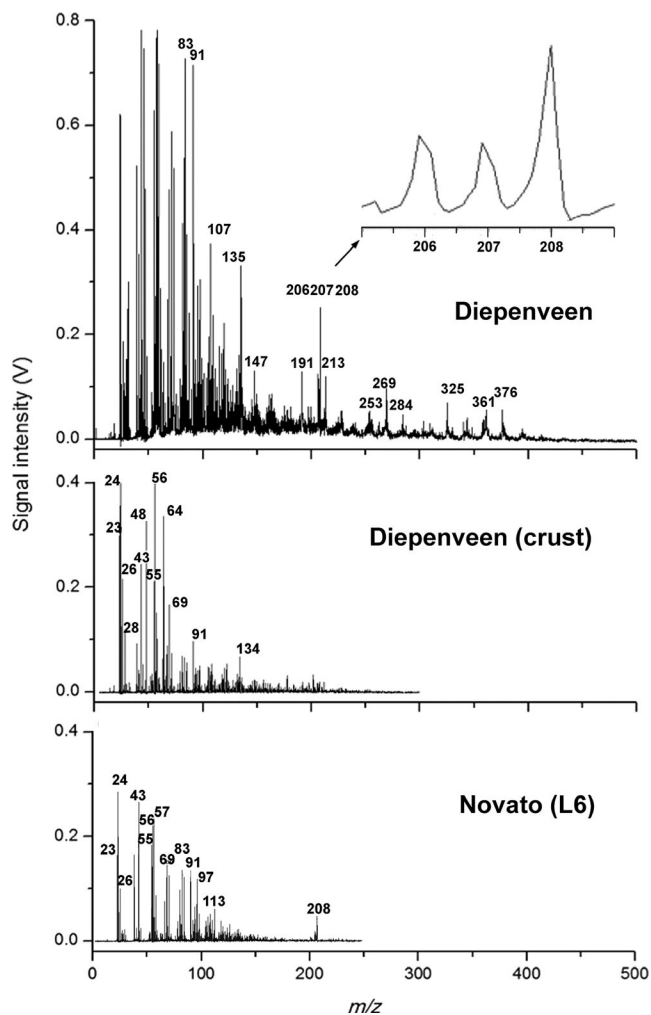


Fig. 15. Diepenveen PAH signature from an aliquot taken inside the meteorite is compared to a signal from the meteorite's fusion crust sample (possibly more contaminated) and the signal for the Novato ordinary chondrite measured under the same conditions (Jenniskens et al. 2014). PAH = polycyclic aromatic hydrocarbon.

(Table 7). Other amino acids detected in Diepenveen, however, are much less easily explained as contamination. These include many four-carbon, aliphatic primary amino acids including DL- $\alpha$ - and DL- $\beta$ -amino-*n*-butyric acids,  $\alpha$ - and DL- $\beta$ -aminoisobutyric acid, in addition to several five-carbon amino acids that are rare or absent in biology (Table 7).

Besides L-glutamic acid, the three most abundant amino acids in Diepenveen are glycine,  $\beta$ -alanine, and  $\gamma$ -amino-*n*-butyric acid (Table 7). Because glycine is a proteinogenic amino acid, it is likely that at least some portion of this amino acid is contamination;  $\beta$ -alanine and  $\gamma$ -amino-*n*-butyric acid also show up in biology,

Table 7. Summary of the total (free + bound) amino acid abundances<sup>1</sup> in the acid-hydrolyzed, hot-water extract of the CM2 Diepenveen, compared with published values for the CM2 Murchison (Burton et al. 2014a).

Amino acid	Diepenveen	Murchison
D-aspartic acid	69 ± 11	120 ± 16
L-aspartic acid	203 ± 3 <sup>6</sup>	132 ± 15
D-glutamic acid	296 ± 22	343 ± 44
L-glutamic acid	2060 ± 80 <sup>6</sup>	357 ± 22
D-serine	93 ± 29	48 ± 9
L-serine	291 ± 15 <sup>6</sup>	46 ± 9
D-threonine	1.0 ± 0.4	–
L-threonine	185 ± 38 <sup>6</sup>	–
glycine	674 ± 109 <sup>6</sup>	1995 ± 122
$\beta$ -alanine	1,040 ± 200	1419 ± 157
D-alanine	85 ± 19	623 ± 6
L-alanine	237 ± 102 <sup>6</sup>	659 ± 84
$\gamma$ -aminobutyric acid	2070 ± 380	1460 ± 213
D- $\beta$ -aminobutyric acid	18 ± 2	233 ± 17
L- $\beta$ -aminobutyric acid	13 ± 7	256 ± 15
$\alpha$ -aminoisobutyric acid	23 ± 7	3182 ± 620
D,L- $\beta$ -aminoisobutyric acid <sup>3</sup>	229 ± 103	–
D,L- $\alpha$ -aminobutyric acid <sup>3</sup>	13 ± 4	403 ± 156
D,L-norvaline <sup>3</sup>	3.0 ± 0.3	37 ± 4
D-isovaline	4.3 ± 0.5	993 ± 443
L-isovaline <sup>4</sup>	>1.1	1444 ± 66
D-3-aminopentanoic acid	3.5 ± 0.4	37 ± 4 <sup>5</sup>
L-3-aminopentanoic acid	2.1 ± 0.2	–
D,L- and allo-3-amino-2-methylbutanoic acid <sup>2</sup>	<0.1	26 ± 5
3-amino-3-methylbutanoic acid	<3.53	<14
3-amino-2,2-dimethylpropanoic acid	4.2 ± 0.4	36 ± 3
D,L-3-amino-2-ethylpropanoic acid <sup>3</sup>	<0.1	37 ± 2
D,L-4-aminopentanoic acid <sup>2</sup>	12 ± 1	84 ± 12
D,L-4-amino-2-methylbutanoic acid <sup>2</sup>	<0.1	67 ± 8
D,L-4-amino-3-methylbutanoic acid <sup>2</sup>	4.1 ± 0.5	103 ± 7
$\delta$ -aminovaleric acid	205 ± 27	50 ± 5
D-valine	14 ± 1	105 ± 15
L-valine	196 ± 20 <sup>6</sup>	111 ± 28
$\epsilon$ -aminocaproic acid	698 ± 146 <sup>6</sup>	268 ± 123
Total:	~8800	~14,000

<sup>1</sup>Values are reported in parts-per-billion based on the bulk sample mass. Uncertainties were calculated from the standard error based on the number of separate measurements. Coeluting peaks and/or compounds with interfering peaks were not included in the average. Upper limits are presented for amino acids that were not present at levels above the procedural blank background levels.

<sup>2</sup>Enantiomers could not be separated under the chromatographic conditions.

<sup>3</sup>Enantiomers could be separated, but not identified, due to a lack of optically pure standards.

<sup>4</sup>There was an interference in the mass chromatogram for L-isovaline that suppressed ion formation, so only a lower estimate is given.

<sup>5</sup>Sum of D- and L-enantiomers; – = not reported.

<sup>6</sup>Likely at least in part a contaminant.

though to a lesser extent. For comparison, in a terrestrial soil sample the ratio of glycine:  $\beta$ -alanine:  $\gamma$ -amino-*n*-butyric acid were measured to be 1:0.2:0.1, whereas in Diepenveen the ratio of these amino acids is 1:1.3:2.2 (Burton et al. 2014a). The significantly higher relative abundances of  $\beta$ -alanine and  $\gamma$ -amino-*n*-butyric acid over glycine (even assuming all of the glycine is indigenous), suggest that the  $\beta$ -alanine and  $\gamma$ -amino-*n*-butyric acid in this meteorite are predominantly indigenous. Compound specific isotopic ratios (e.g.,  $^{13}\text{C}/^{12}\text{C}$ ,  $^{15}\text{N}/^{14}\text{N}$ ) are needed to firmly establish the origin of these amino acids however, insufficient sample mass was available to make these measurements. Also present in the sample is an abundance of  $\epsilon$ -amino-*n*-caproic acid, the product of the hydrolysis of nylon 6.

That this amino acid is primarily in the acid hydrolyzed, or “bound” as opposed to the unhydrolyzed or “free” form is consistent with nylon contamination (Glavin et al. 2006).

The methanol-soluble organic fractions of Diepenveen analyzed using high-field Fourier transform ion cyclotron mass spectrometry (ICR-FT/MS) in negative electrospray ionization mode (ESI<sup>-</sup>) had only 945 assigned mass peaks. Figure 16, for example, shows the Diepenveen soluble organic matter in the mass range from 354.90 to 355.35  $m/z$ . Arrows indicate the mass difference  $\Delta m = 36.4$  mDa, corresponding to regular compositional series and a nominal exchange of O versus  $\text{CH}_4$ . Figure 17 shows the data visualized in a van Krevelen diagram, in terms of the H/C ratio

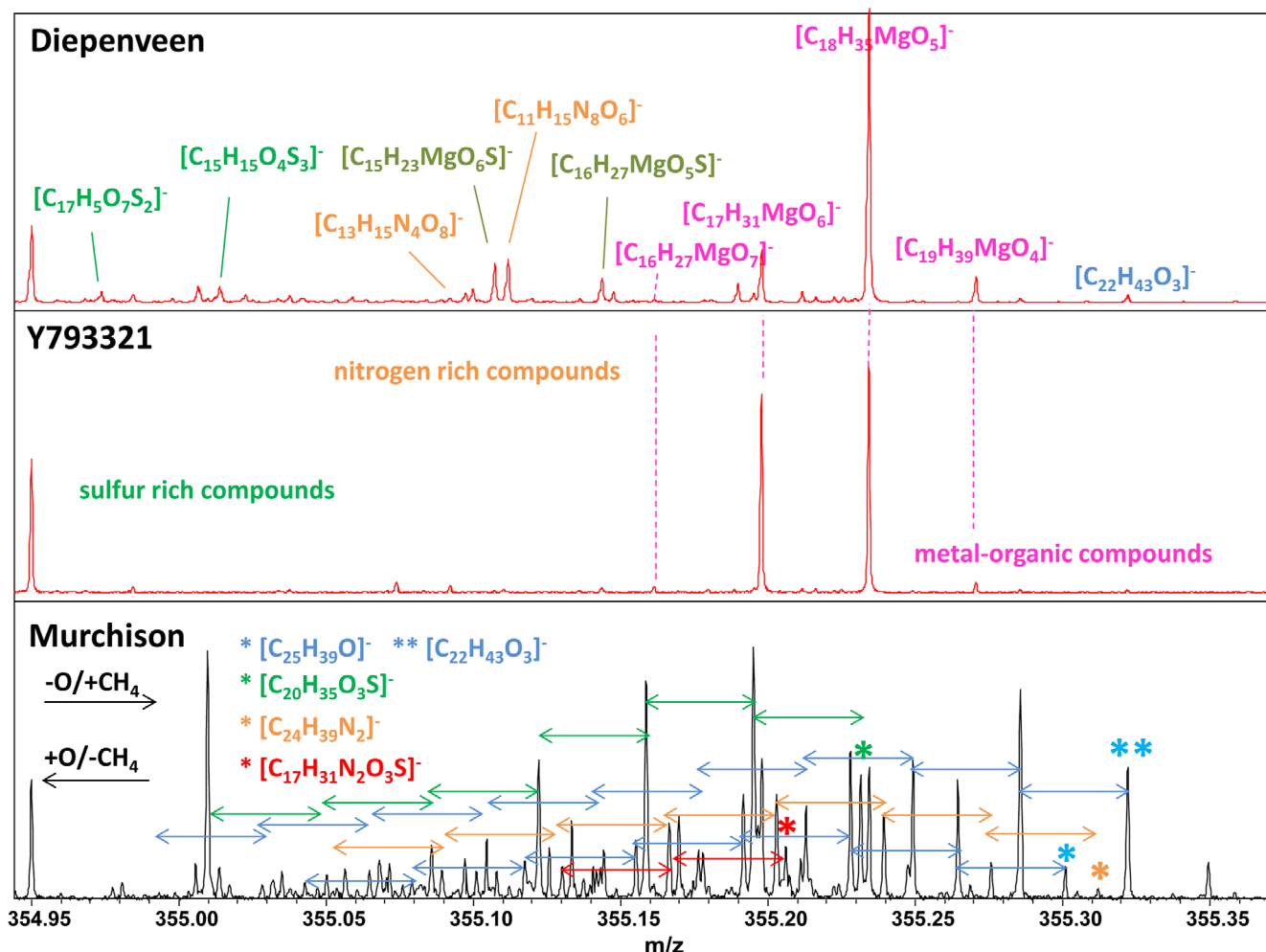


Fig. 16. Details on molecular ions  $[\text{MH}^-]$  with nominal mass  $m/z = 355$ , showing elementary formula annotations in the CHNOSMg space. Diepenveen and Y793321 show intense CHOMg compounds and a loss of the complex and regular chemical signature such as present in the Murchison CM2 with homologous CHO, CHOS, CHNO, and CHNOS molecular series. Arrows indicate the mass difference  $\Delta m = 36.4$  mDa, corresponding to a nominal exchange of O versus  $\text{CH}_4$ . (Color figure can be viewed at [wileyonlinelibrary.com](http://wileyonlinelibrary.com).)

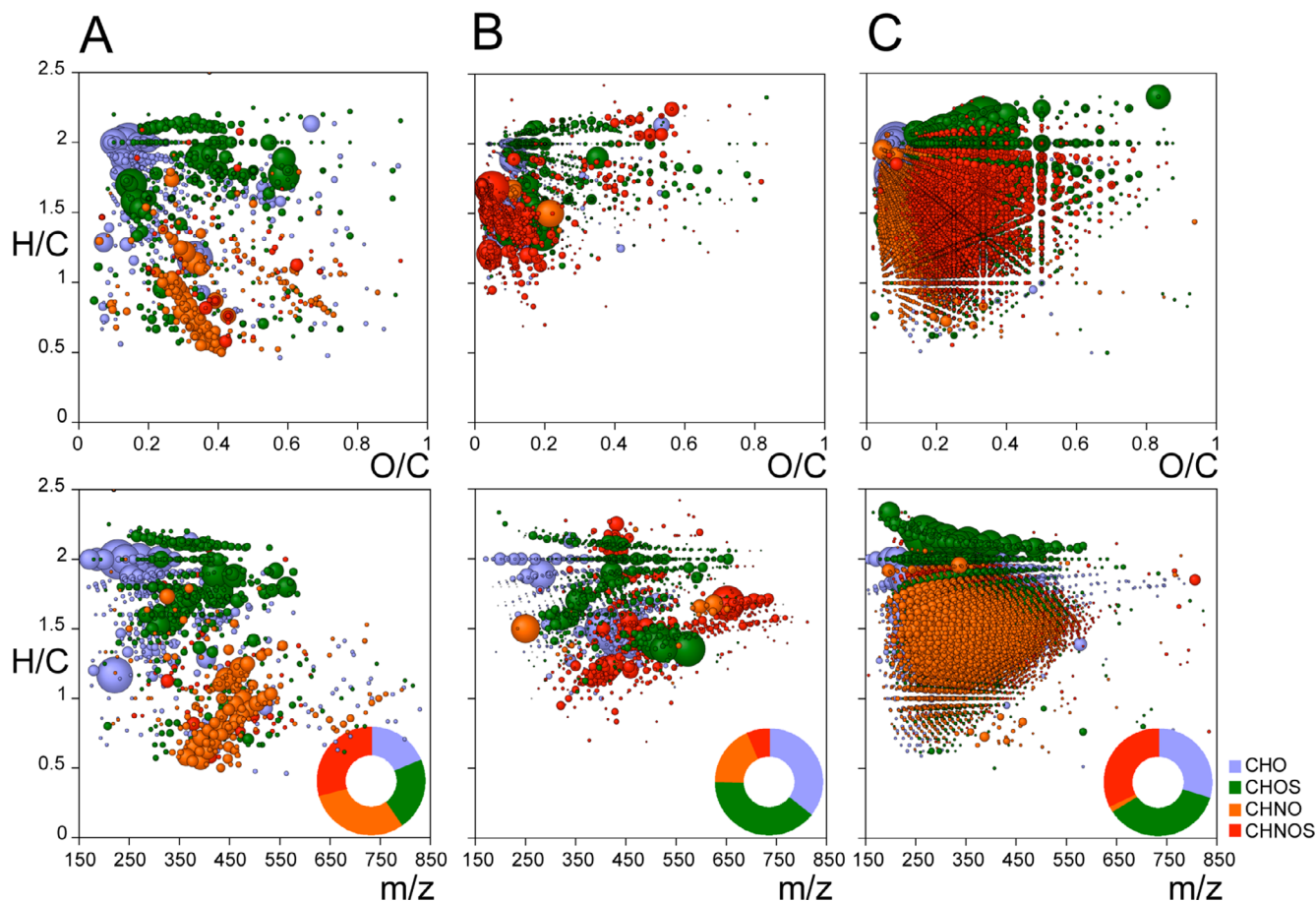


Fig. 17. Negative electrospray ICR-FT/MS data visualized as (top) van Krevelen H/C versus O/C and (bottom) mass edited H/C ratio of (A) Diepenveen, (B) Y 793321, and (C) Murchison. Insert histograms show the percentage of all assigned molecular formulas according to the color codes, namely CHO (blue), CHOS (green), CHNO (orange), and CHNOS (red). Bubble areas indicate relative mass peak intensity of each ion. The regular chemical space typical of pristine CM2 such as Murchison soluble organics is heavily altered in Diepenveen and Y793321. (Color figure can be viewed at [wileyonlinelibrary.com](http://wileyonlinelibrary.com).)

versus O/C (top) and the mass edited H/C ratio versus molecular mass over charge  $m/z$  (bottom). An inset histogram shows the percentages of the respective molecular series: CHO (36.0%), CHOS (39.5%), CHNO (18.4%), and CHNOS (6.4%). Only a few signals in each nominal mass could be assigned mainly to sulfur-rich and organo-magnesium compounds. Organo-magnesium compounds were found recently as indicators of thermal metamorphism, i.e., are almost not seen in very pristine material but highly abundant in higher temperature altered materials (Ruf et al. 2017).

Figure 18 shows the calculated aromaticity equivalent  $X_c$ , defined recently as a new parameter calculated from the assigned molecular formulas to better characterize the aromatic and condensed aromatic compounds (Yassine et al. 2014).  $X_c$  is complementary to the aromaticity index and is calculated

from  $X_c = (3 \cdot [DBE - (mN_O + nN_S)] - 2) / (DBE - [mN_O + nN_S])$ , where DBE is the double-bond equivalent and  $m$  and  $n$  correspond to the fraction of oxygen ( $N_O$ ) and sulfur ( $N_S$ ) atoms involved in  $\pi$ -bond structures of a compound (Kourtchev et al. 2016). Based on values of  $0 \leq X_c < 2.5$ , 20.8% of detected molecules in Diepenveen's methanol-soluble extract are condensed aromatic and aromatic compounds containing benzene rings, while 79.2% are acyclic and cyclic compounds without benzene rings ( $2.5 \leq X_c \leq 3.0$ ).

## DISCUSSION

### Circumstances of the Fall

Local and regional periodic publications were searched, but no account related to the Diepenveen fall was found, despite the fact that, following the

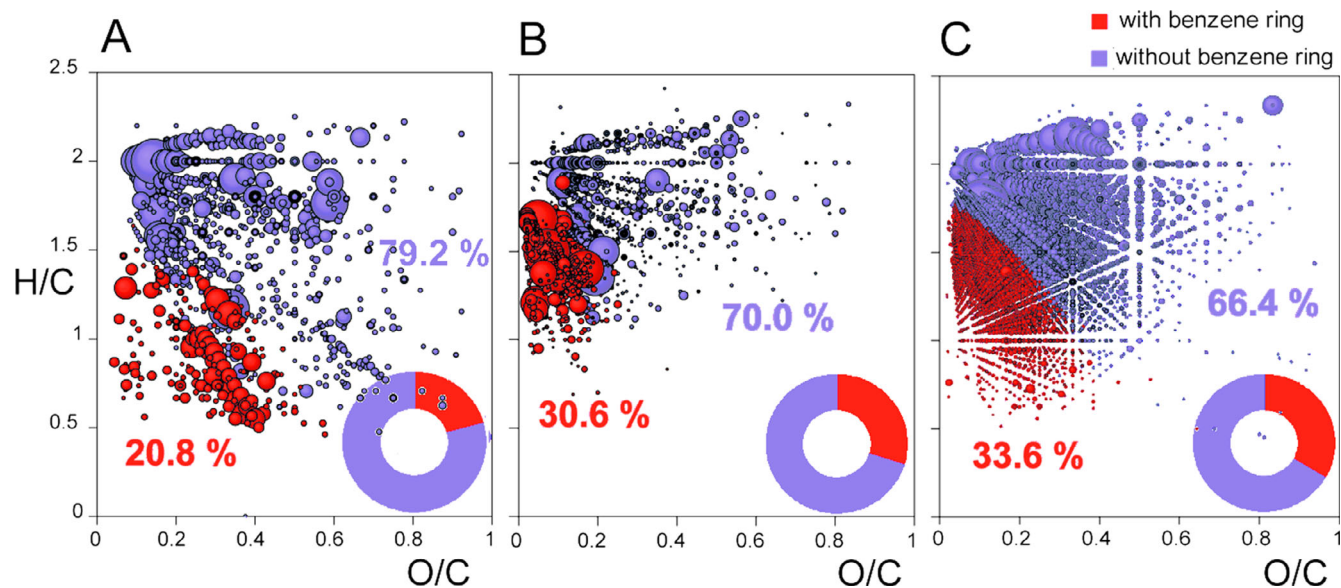


Fig. 18. As Fig. 10, Van Krevelen diagrams of sorted H/C versus O/C based on the application of the calculated aromaticity equivalent  $X_c$  derived from the negative electrospray ICR-FT/MS data ( $0 \leq X_c \leq 3$ ;  $m = 1$  and  $n = 1$ ) of (A) Diepenveen, (B) Y 793321, and (C) Murchison. Molecular series highlighting acyclic and cyclic (without benzene ring) compounds are colored in blue ( $0 \leq X_c < 2.5$ ), whereas molecular series of the condensed aromatic and aromatic (with a single benzene ring) compounds are colored in red ( $2.5 \leq X_c \leq 3$ ). Bubble areas indicate relative mass peak intensity of each ion. (Color figure can be viewed at [wileyonlinelibrary.com](http://wileyonlinelibrary.com).)

spectacular 1866 Leonids and the 1872 Andromedids storms over Europe, meteor sightings were frequently reported in those days (e.g., Walker 1874; Heis 1877).

The weather did not completely hinder observations. The atmospheric conditions in the week of the fall were reconstructed based on historical meteorological records. Each day, observations were made at 8 A.M., 2 P.M., and 8 P.M. local solar time. Figure 2 provides the weather map constructed from the 2 P.M. observations. In the afternoon of October 27, 1873, a moderate northerly flow was advecting slightly unstable polar air with good visibilities at the eastern flank of a high-pressure system over the British Isles. In this situation, clouds tend to consist of cumulus with some stratocumulus-sheets above. The skies were partly cloudy, locally mostly cloudy, with mainly dry weather. Conditions gradually improved during the afternoon. In the evening, the clearances were widening and inland the skies became mostly clear. In a partially cloudy sky, a daytime fireball could have been seen.

With no public records announcing the fall, the meteorite remained anonymous, perhaps aided by a note added at the top of the box (Fig. 1a). The label reads: “See: meteorite of Orgueil, *Album der Natuur* 1883, p. 89.” The “*Album der Natuur*” was a popular-scientific periodical that was well-read by school teachers at that time. In the 1883 volume is an article by Krecke, “*De Meteorsteenen*” (“the Meteor Stones”).

It contains a description and illustration of Orgueil, a CI (Ivuna-like) carbonaceous chondrite that fell in France in 1864. Geochemical analysis confirms Diepenveen is not Orgueil (Langbroek et al. 2015).

Comparisons of handwriting reveal that this small note might have been written by Jan Sirks, who was the physics teacher of D. H. te Wechel. Sirks was known for his outreach activities in Deventer, also to laymen, and made use of the school’s collection of specimens and demonstration tools. He might also be the manufacturer of the box in which the Diepenveen was stored.

### Classification

Since this meteorite contains thermally metamorphosed clasts, and is a breccia, it cannot be usefully classified using the scale proposed by Rubin et al. (2007). The phyllosilicate fraction, proposed as a measure of aqueous alteration (Howard et al. 2015; King et al. 2017), varies considerably from clast to clast and is difficult to measure accurately. The abundance of metal, another criterion for classification, varies from lithology to lithology. The abundance of coarse-grained tochilinite-serpentine aggregates has been obscured by brecciation. Surviving, unbrecciated clasts (see Fig. 4) indicate that the abundance of these aggregates probably varies considerably. The olivine’s relatively

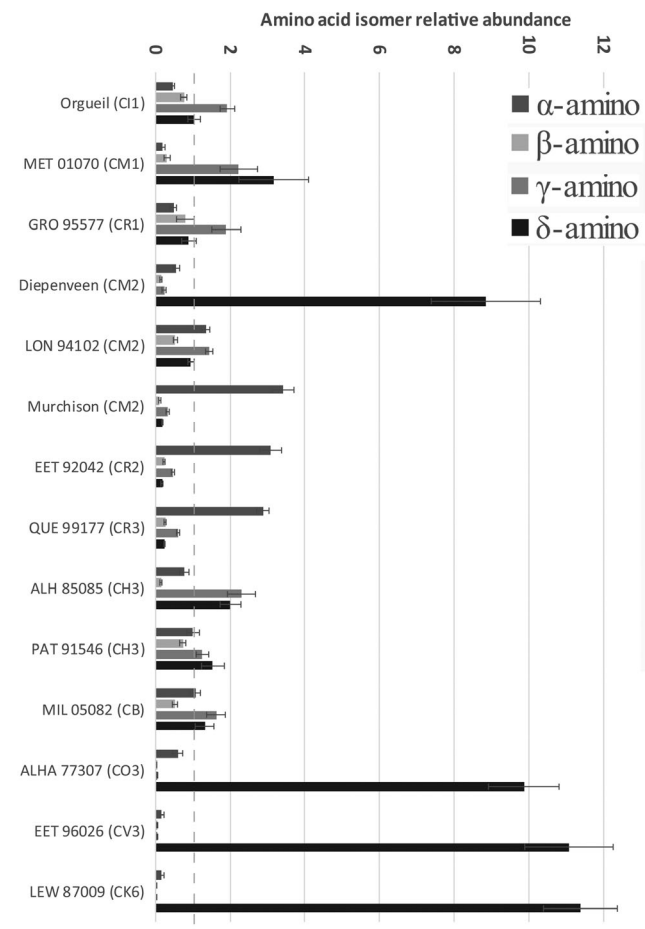


Fig. 19. Comparison of the relative molar abundances of the C5 amino acids in carbonaceous chondrites as a function of amine position ( $\alpha$ -,  $\beta$ -,  $\gamma$ -, and  $\delta$ -). All amino acid data (except for Diepenveen) taken from Burton et al. (2012, 2013, 2014a, 2014b, 2015) and Glavin et al. (2006, 2010).

high abundance suggests an overall low degree of aqueous alteration; however, complex carbonates (dolomite) are observed that suggest the opposite conclusion.

Diepenveen is a highly brecciated CM chondrite, and probably contains material spanning the entire range of proposed CM subtypes (Rubin et al. 2007). In contrast, Paris contained principally only two subtypes and an average subtype of CM2.7 could be suggested by Hewins et al. (2014). Because the situation for Diepenveen is much more variable, we refrain from assigning a single CM subtype.

The petrography and mineralogy of Diepenveen is that of a CM chondrite which in places experienced significant but clearly variable aqueous alteration. Rather than being mildly heated, Diepenveen is less aqueously altered there. The evidence for this includes the variable presence of Fe,Ni metal and the relatively low probe total deficits measured in matrix at places, where oxygen and

hydrogen are not being counted (which at first glance appears to be evidence of heating), but there are also widespread tochilinite (Fig. 4D) and small clusters of phyllosilicates (Fig. 4B). There are no olivine pseudomorphs after phyllosilicates, which would be expected from heating. Some euhedral, relatively Fe-rich (Fa80) olivine grains have been observed in the matrix.

The water content of Diepenveen is similar to the 9–14 wt% (10.5 wt% average) of other CM meteorites (Jarosewich 1990; Piani et al. 2018). The EPMA mass balance including water is more realistic in view of the 53 vol% matrix, which consists mainly of tochilinite and serpentine. In this balance, tochilinite and serpentine represent 44.8 vol% of the bulk rock, which corresponds to ~84 vol% of the matrix, the remainder being small olivine fragments. At an average 12 wt% water (hydroxyl) in the mineral structure, tochilinite and serpentine alone can thus explain about 10 wt% of water in the matrix.

Shock pressure can flatten grain assemblies, which would result in an alignment of mineral clasts. While there is some alignment in the general orientation of components within clasts, like that shown in Fig. 4A, suggestive of impact deformation that was correlated with higher levels of aqueous alteration (Rubin 2012), there is no such alignment in the assembly (Fig. 4F).

### Oxygen Isotope Mixing Lines

It is a puzzling aspect that highly aqueously altered CMs have similar O isotopes as do the less altered ones. Aqueous alteration is thought to have occurred early in the history of the parent body, about 4.563 Ga ago (Fujiya et al. 2012; Lee et al. 2014), perhaps on just one CM chondrite parent body (Lindgren et al. 2017). While the body was cooling, water that was being incorporated into the hydrated minerals changed its  $^{17}\text{O}$  and  $^{18}\text{O}$  abundance relative to  $^{16}\text{O}$ . Different types of minerals are found at different locations in the three-isotope diagram (Fig. 9), with carbonates at highest  $\delta^{18}\text{O}' = 20\text{--}40\text{‰}$ , hydrous minerals at intermediate  $\delta^{18}\text{O}' = 5\text{--}20\text{‰}$ , and anhydrous minerals at the lowest  $\delta^{18}\text{O}' < 10\text{‰}$  (Young 2001). Mixing lines are thought to arise because the component minerals are formed at different locations or at different times.

Based on petrographic analysis of other CM chondrites, the last phases to be attacked by fluids were Mg-rich olivines and pyroxenes in chondrules with low  $\Delta^{17}\text{O}'$  values ( $-3$  to  $-7\text{‰}$ ) (Chaumard et al. 2018). If so, fluids from which the phyllosilicates formed during the last stages of alteration were isotopically  $^{16}\text{O}$ -rich (King et al. 2018).

The Diepenveen oxygen isotopes plot among hydrous and anhydrous minerals (Fig. 9), consistent

with a lack of carbonates. All samples in the 2nd and 3rd aliquot of Diepenveen studied (with values  $\delta^{18}\text{O} < 0$ ) are distributed along a line in the anhydrous  $^{16}\text{O}$ -rich part of the diagram with a slope  $\delta^{17}\text{O}'/\delta^{18}\text{O}' = 0.85 \pm 0.05$  (dashed line in Fig. 9). The slope is less steep than the Young & Russell slope of 1.00 (Young and Russell 1998), the primitive chondrule minerals (PCM) slope of  $0.987 \pm 0.013$  (Ushikubo et al. 2012; Chaumard et al. 2018), defined by chondrules in relatively pristine carbonaceous chondrites, or even the carbonaceous chondrite anhydrous mineral (CCAM) slope of  $0.94 \pm 0.01$  (Clayton and Mayeda 1999).

The Diepenveen line connects the average value of Murchison anhydrous separates with one of the 'Initial CM water' reservoir at  $\delta^{18}\text{O}' = +28$ ,  $\delta^{17}\text{O}' = +18\text{‰}$ , proposed by Clayton and Mayeda (1999) (star in Fig. 9) and the  $\delta^{18}\text{O}' = +2.0$ – $8.1$ ,  $\delta^{17}\text{O}' = -1.0$ – $3.0\text{‰}$  fluid from which carbonates were aqueously altered at 20–71 °C in Murchison, measured by (Guo and Eiler 2016). Many other meteorites in this space were classified as "C-ungrouped" (+ in Fig. 9).

A second trend line (short dashed line in Fig. 9) is more or less parallel to the first with a slope  $\delta^{17}\text{O}'/\delta^{18}\text{O}' \sim 0.85$  but plots  $-2\text{‰}$  lower in  $\delta^{17}\text{O}'$ . Five samples of the first batch of Diepenveen aliquots are found along this line.

One aliquot from the first set of measurements plots along the first line, but also at a position  $\delta^{18}\text{O}' = +5.8$  where it plots among samples labeled as "dehydrated CM" (orange squares in Fig. 9, data from Clayton and Mayeda 1999) and the highly aqueously altered CM1 and CM1/2 samples (petrologic subtype 1.2 and 1.1) studied recently by King et al. (2018), which scattered along a slope  $0.48 \pm 0.04$  (however, previously measured CM1 and CM1/2 samples scattered along the entire CM2 range). At this point, the slope becomes shallower, and aligns with non-acid-treated CM chondrite Sutter's Mill SM43 (Jenniskens et al. 2012), and one aliquot of SM12 (Fig. 9).

An alternative explanation for the first set of Diepenveen samples is that this group is aligned along a similar shallow slope, and forms an extension of the trend line seen among Sutter's Mill SM3 samples above  $\delta^{18}\text{O}' = +10\text{‰}$  (solid line in Fig. 9). If so, it would extend this trend to  $\delta^{18}\text{O}' = +5\text{‰}$ , as far down as the Clayton and Mayeda (1999) sample of dehydrated CM. This trend has a more shallow slope  $\delta^{17}\text{O}'/\delta^{18}\text{O}' = 0.60 \pm 0.03$  (Jenniskens et al. 2012), slightly steeper than the terrestrial mass-dependent fraction line (TFL). For Paris (Hewins et al. 2014; Vacher et al. 2017) and other CMs for which many aliquots were measured, oxygen isotopes of individual aliquots also spread along a slope of  $\sim 0.62$ , but they show different vertical displacements in  $\delta^{17}\text{O}'$ . Noncarbonate samples

of Paris, the least altered CM chondrite known to date (Hewins et al. 2014; Rubin 2015; Verdier-Paoletti et al. 2017), plot in the same range of  $\delta^{18}\text{O}'$  but  $\delta^{17}\text{O}' = 0.7\text{‰}$  lower than the samples by Clayton and Mayeda (1999), while Diepenveen plots  $\delta^{17}\text{O}' = 1.6\text{‰}$  lower.

Diepenveen shares the position at this slightly lower  $\delta^{17}\text{O}'$  (and low  $\delta^{18}\text{O}'$ ) end with a small number of unusual Antarctic CM meteorites Y-793321 and A-881334 (Clayton and Mayeda 1999) and A-881458 (Nakamura 2006), of which Y-793321 and A-881458 are also regolith breccias. Y-793321 shows mild thermal metamorphism in FeNi metal grain properties (category B), while A-881458 does not (category A) (Kimura et al. 2011). Y-793321 and A-881334 are also known to have distinctly different  $\delta^{13}\text{C}_{\text{bulk}}\text{-}\delta\text{D}$  isotopes (Oba and Naraoka 2009).

This subgroup is thought to be the product of thermal metamorphism (Tonui et al. 2014; Lee et al. 2018), whereby heating after hydration resulted in dehydroxylation and recrystallization of phyllosilicates. The O isotopes of metamorphosed CMs are heavier than unmetamorphosed CMs (Tonui et al. 2014), which would move the samples to higher  $\delta^{17}\text{O}'$  and  $\delta^{18}\text{O}'$ . In Diepenveen, this process must have been mild, because the heavy isotope abundances are still low.

In summary, Diepenveen must have been aqueously altered relatively late in the life of the CM parent body, having been altered by relatively  $^{16}\text{O}$ -rich water, affecting some parts more than others. This alteration was followed by mild thermal metamorphism.

## Chemistry of Organic Compounds

Other insight in the role of aqueous alteration and thermal metamorphism comes from the organic matter in the meteorites. Diepenveen has several unusual aspects to its amino acid content. The  $\beta$ -alanine to glycine ratio of Diepenveen at 1.95 is closer to that typical of CI chondrites ( $\sim 2$ – $3$ ) than to CM chondrites ( $\sim 0.5$ ) (Burton et al. 2014a) and indicates that the fragment analyzed experienced significant parent body alteration under mildly warmer temperatures than typical for CM chondrites. In comparison, the least known aqueously altered, and only weakly affected by thermal metamorphism CM chondrite Paris, had a ratio of 0.15 (Martins et al. 2015).

A comparison of the relative molar abundances of the amino acids shows that the straight chain terminal amine ( $n$ - $\omega$ ) isomer is the most abundant not only for  $\epsilon$ -amino- $n$ -caproic acid but also the three-, four-, and five-carbon amino acids. The propensity for  $n$ - $\omega$  amino acids has been observed in thermally altered meteorites, including CO, CV, CK, the CM Sutter's Mill, and in

thermally altered CIs (Burton et al. 2012, 2014a, 2014b, 2015), though in those cases the *n*- $\omega$  amino acids were primarily in the “free” form. The ratio of five-carbon amino acids based on amine position ( $\alpha$ -,  $\beta$ -,  $\gamma$ -, and  $\delta$ -) has been shown to correlate with mineralogy and parent body alteration (e.g., Elsila et al. 2016). In Diepenveen, the *n*- $\omega$   $\delta$ -aminovaleric acid dominates with much lower, but detectable, abundances of  $\alpha$ -,  $\beta$ -, and  $\gamma$ - C5 amino acids.

This distribution of C5 amino acids in Diepenveen is much more similar to the thermally altered CO and CV chondrites, rather than other CM2 meteorites which are dominated by  $\alpha$ -amino acids (Fig. 19). The dashed line on the *y*-axis of Fig. 19 corresponds to the expected relative abundance if the amino acids were formed by a completely nonselective synthetic process. The predominance of  $\delta$ -aminovaleric acid (5-aminopentanoic acid, 5-apa) relative to other C5 amino acids in Diepenveen is similar to the distributions found in thermally altered CO, CV, and CK chondrites. However, like CM2 meteorites, there is more amino acid structural diversity in Diepenveen (Table 7). The presence of structural diversity and of higher abundances of typical of CM2 meteorites (e.g., Murchison) but with a higher fraction of *n*- $\omega$  than of  $\alpha$ - amino acids, suggest that Diepenveen is an unusual CM2 meteorite. Results are consistent with the conclusion that the meteorite has experienced some thermal alteration on the parent body.

Compared to Murchison, Diepenveen showed much lower molecular compositional diversity in the methanol-soluble fraction (Fig. 17). Murchison (7257 assigned mass peaks) showed a dense and contiguous occupancy of the CHNOS chemical space, with a remarkable diversity of molecular compositions and classes of structures (Schmitt-Kopplin et al. 2010).

Y-793321 showed a mass spectrum (Fig. 17) similar to that of Diepenveen with a slightly elevated diversity of identified molecular compositions (1651 assigned mass peaks) and relatively higher proportions of sulfur compounds, namely CHOS (36.3%) and CHNOS (32.5%) at the expense of CHO (29.8%) and CHNO (1.6%) molecular compositions. Interestingly, Y-793321 still showed a low intensity background mass peak signature of considerable diversity, which had fully disappeared in Diepenveen soluble organic matter as shown in the mass range from 342.900 to 343.345 *m/z* (Fig. 16).

Based on the calculated aromaticity equivalent  $X_c$ , Diepenveen seems more affected by alteration than Y-793321 (Fig. 18), compared to Murchison, with few more very condensed nitrogen containing aromatic structures and mainly higher abundance of aliphatic structures. Thermal alteration by heating or radiation can change the signatures of Murchison toward the

signature of Diepenveen (Ruf et al. 2017). This result agrees with Vinogradoff et al. (2017), who found that hydrothermal alteration induced aromatization and oxidation of the insoluble organic matter, as well as a decrease in radical and nitrogen content.

In summary, organic compounds in Diepenveen show evidence of alteration by heating or radiation. This alteration may have occurred before the organic material was incorporated into the mineral assemblages, with subsequent aqueous alteration and thermal metamorphism only mildly affecting the functional groups and aromatic structure.

### Collisional History and Origin Region

Some of the “C-ungrouped” and dehydrated CM meteorites have young  $\sim 1.3$ – $2.8$  Ga K-Ar ages (Turrin et al. 2014), like the  $\sim 1.5$  Ga of Diepenveen, suggesting the thermal metamorphism in Diepenveen could have occurred in impacts late in the history of the solar system.

The noble gas inventory in Diepenveen bears some resemblance to the ones of two other dehydrated CM regolith breccias, Antarctic meteorites Y-793321 and A-881458 (Nakamura 2006). The solar wind concentration for Diepenveen is an order of magnitude lower than in Y-793321, but similar to A-881458 (Fig. 12, inset). The  $^{40}\text{Ar}$  concentrations of Y-793321 and A-881458 are similar at  $\sim 9 \times 10^{-6} \text{ cm}^3\text{STP g}^{-1}$ , and assuming a typical K concentration of 400 ppm (Wasson and Kallemeyn 1988), results in a K-Ar age of 2.6 Ga, significantly higher than for Diepenveen ( $\sim 1.1$  Ga). So while there are some similarities between the noble gas inventories of Diepenveen and the two other dehydrated CM regolith breccias, we cannot firmly conclude that they originated from the same impact event or parent body.

Two CM chondrites, Sutter’s Mill and Maribo, were tracked while moving through Earth’s atmosphere from which an orbit was calculated. Both arrived on eccentric orbits with a perihelion near Mercury and a semimajor axis still close to the delivery 3:1 mean-motion resonance with Jupiter (Jenniskens et al. 2012), suggesting CM chondrite meteoroids do not survive long enough to evolve the semimajor axis of their orbits significantly from close encounters with the terrestrial planets. Indeed, 90% of CM chondrites have CRE ages less than 2 Ma (Eugster et al. 2006).

Sutter’s Mill (and Maribo) travelled through the atmosphere with a fast  $28 \text{ km s}^{-1}$  entry speed, and only  $\sim 1$  kg from a large 3 m ( $\sim 30,000$  kg) meteoroid survived (Jenniskens et al. 2012). In contrast, Diepenveen fell from a small  $\sim 30$  cm sized meteoroid with a mass of 30 kg, if the meteoroid had the same density as the 68 g surviving meteorite. Ablation was a factor of  $>68$  times



less efficient. This implies a smaller entry velocity, suggesting a perihelion of the orbit closer to Earth's orbit, like Murchison (Halliday and McIntosh 1990). If its orbital evolution did not bring it closer to the Sun than Earth, this may have allowed the meteoroid to survive interplanetary space longer.

The  $4\pi$  CRE age of  $\sim 5$  Ma for Diepenveen is higher than for many other CM chondrites, which fall in three clusters at  $\sim 0.2$  Ma, 0.6 Ma, and 1–3 Ma ages (e.g., Nishiizumi and Caffee 2012). While there are some similarities between the cosmogenic and trapped noble gas inventories of Diepenveen and the two other dehydrated CM regolith breccias, which all have relatively long  $4\pi$  exposure ages between 3 and 10 Ma, we cannot firmly conclude that they originated from the same impact event on the CM chondrite parent body.

Meier et al. (2016) suggested that the group of 3–10 Ma old meteorites originated from the  $8.3 \pm 0.5$  Ma breakup of the Veritas family (Nesvorný et al. 2003), but this family of asteroids is located in the outer Main Belt (Michel et al. 2010). Meteoroids generated in the outer Main Belt tend to evolve into Jupiter-crossing orbits and are ejected from the solar system, before their perihelion reaches Earth orbit, unless they have an inclination much higher than the Veritas family (Jenniskens 2019).

After ejection, the meteoroid survived collisions for at least 5 Ma. The dynamical age against collisions in the asteroid belt is about  $\tau = 1.4\sqrt{R}$ , with  $R$  the radius of the meteoroid in cm and  $\tau$  given in millions of years (Wetherill 1985), possibly underestimated by a factor of 3–5 (Jenniskens et al. 2014). This translates to about  $\tau = 5$  Ma for a 30 cm sized object or  $\tau = 17$  Ma for a 3 m sized meteoroid. That means Diepenveen's origin site in the asteroid belt is not constrained by the lifetime against collisions (Jenniskens et al. 2019).

### Implications for Future Sample Return

As the constituting particles of the powder are comparable or smaller than the length scale of the lithic elements comprising the matrix of Diepenveen, the powdered aliquot is a suitable analog for the fine-grained textures of asteroidal regolith.

Diepenveen's reflectance spectrum falls within the spectral variation of Cg-type asteroid and Hayabusa2 mission target (162173) Ryugu (Fig. 11). Figure 11A shows disk-integrated spectra at different rotational phases (Binzel et al. 2002; Vilas 2008; Lazzaro et al. 2013). The asteroid has a rotational period of  $7.63 \pm 0.01$  h (Müller et al. 2011). The geometric albedo of Ryugu is about 0.047 (Le Corre et al. 2018). The overall featureless spectrum of Ryugu has been

shown to vary in UV absorption (Lazzaro et al. 2013), near-IR slope (Perna et al. 2017; Le Corre et al. 2018) and the intensity of the absorption at  $0.7 \mu\text{m}$  (Vilas 2008).

Studies of suitable meteorite analogs for Ryugu suggest that unusual or heated CM and CI carbonaceous chondrites may be best-fitting to the asteroid's spectral characteristics (Perna et al. 2017; Kitazato et al. 2019). Diepenveen belongs to this class and might provide an indication of what the samples of Ryugu returned by Hayabusa2 will look like.

Interestingly, the presence of hydrated minerals and magnetite in Diepenveen may also suggest a relationship with B-type asteroid (101955) Bennu (Hamilton et al. 2019), even though the Diepenveen reflectance spectrum is not a good match to that of B-type asteroids (Fig. 11).

## CONCLUSIONS

The carbonaceous chondrite Diepenveen is a petrographically CM-like regolith breccia poor in solar wind implanted noble gases. Compared to regular CM chondrites, it is unusual in several aspects of its mineralogy and organic composition, its oxygen isotopes, and CRE age. Contamination from handling since its recovery in 1873 is minor, with no significant increase of Na or K, but D/L ratios of common amino acids of order 0.01–0.35, instead of the expected 0.5 in an intrinsic (racemic) mixture.

Diepenveen's oxygen isotopes plot mostly outside the traditional CM range into the regime of anhydrous minerals. Different lithologies experienced varying levels of aqueous alteration processing, being less aqueously altered at places rather than mildly heated. Aqueous alteration occurred in fluids that were isotopically  $^{16}\text{O}$  rich, hence Diepenveen must have aqueously altered relatively late in the life of the CM parent body.

Parts of the meteorite experienced mild thermal alteration, while other parts appear thermally unaltered. In Diepenveen, this process must have been mild, because the heavy oxygen isotope abundances are still low. A small agglutinate grain suggests a regolith setting for Diepenveen, with active impact processing. Alignment in the orientation of components within some clasts is suggestive of impact deformation, but such alignment is not present in the assembly.

The organic matter in Diepenveen shows more evidence of alteration by heat or radiation. Diepenveen's propensity for n- $\omega$  amino acids was previously observed in thermally altered meteorites. A lower compositional diversity of methanol-soluble compounds and fewer nitrogen-containing aromatic

structures also point to thermal alteration. This alteration may have occurred before the organic compounds were associated with the mineral assemblages in which they are found now.

Diepenveen fell to Earth from a small 30 cm sized meteoroid that was liberated from a larger body a relatively long time, ~5 Ma, ago. It was liberated from terrain that experienced small impacts, having a K-Ar age of about ~1.5 Ga.

Diepenveen has oxygen isotopes similar to a subgroup of carbonaceous chondrites previously classified as “C-ungrouped,” which are a match to the reflectance spectrum of asteroid Ryugu. Hence, Diepenveen may provide a pre-view of the samples to be returned by the Hayabusa2 mission.

*Acknowledgments*—We are very grateful to the last owner, Mrs. Leida Kiers, for donating the meteorite to the Dutch state collections curated by Naturalis in Leiden in October 2013. We thank Rhian Jones and Adrian Brearley for facilitating the sample distribution. S.J. d. V. thanks Ruben Abellon for support with the spectral measurements at TU Delft. M. L. was a guest researcher at the VU Department of Earth Sciences during part of this research. L. M. K. acknowledges the thorough analytical work by Hans de Groot and Eric Buter of Naturalis, as well as that by Tilly Bouten using the National Geological Facility electron microscope funded by a FES grant to Naturalis and a NWO large investment grant to Utrecht University. W. v. W. acknowledges financial support of the Netherlands Organization for Scientific Research and the Netherlands Space Office. M. M. M. M. is supported by grants from the Swiss National Science Foundation. A. S. B., D. P. G., and J. P. D. were supported by the NASA Astrobiology Institute and the Goddard Center for Astrobiology, and a grant from the Simons Foundation (SCOL award 302497 to J. P. D.), as well as by NASA’s Planetary Science Research Program. The work was supported in part also by NASA grants NNX14AM62G and NNX16AD34G (Q.-Z. Y.), and by NASA grants NNX14AR92G and 80NSSC18K08 (P. J.).

*Editorial Handling*—Dr. A. J. Timothy Jull

## REFERENCES

- Akin F. J., Snook M. E., Severson R. F., Chamberlain W. J., and Walters D. B. 1976. Identification of polynuclear aromatic hydrocarbons in cigarette smoke and their importance as tumorigens. *Journal of the National Cancer Institute* 5:191–195.
- Alexander C. M. O’D., McKeegan K. D., and Altwegg K. 2018. Water reservoirs in small planetary bodies: Meteorites, asteroids and comets. *Space Science Reviews* 214:36–83.
- Barkan E. and Luz B. 2005. High precision measurements of  $^{17}\text{O}/^{16}\text{O}$  and  $^{18}\text{O}/^{16}\text{O}$  ratios in  $\text{H}_2\text{O}$ . *Rapid Communications in Mass Spectrometry* 19:3737–3742.
- Binzel R. P., Lupishko D. F., Di Martino M., Whiteley R. J., and Hahn G. J. 2002. Physical properties of NEOs. In *Asteroids III*, edited by Bottke F. Jr., Cellino A., Paolocchi P., and Binzel R. P. Tucson, Arizona: University of Arizona Press. pp. 255–271.
- Brearley A. J. and Jones R. H. 1998. Chondritic meteorites. In *Planetary materials*, edited by Papike J. J. Reviews in Mineralogy, vol. 36. Washington, D.C.: Mineralogical Society of America. pp. 3-1–3-398.
- Britt D. T. and Consolmagno G. J. 2003. Stony meteorite porosities and densities: A review of the data through 2001. *Meteoritics & Planetary Science* 38:1161–1180.
- Burton A. S., Elsila J. E., Callahan M. P., Martin M. G., Glavin D. P., Johnson N. M., and Dworkin J. P. 2012. A propensity for *n*-w-amino acids in thermally altered Antarctic meteorites. *Meteoritics & Planetary Science* 47:374–386.
- Burton A. S., Elsila J. E., Hein J. E., Glavin D. P., and Dworkin J. P. 2013. Extraterrestrial amino acids identified in metal-rich CH and CB carbonaceous chondrites from Antarctica. *Meteoritics & Planetary Science* 48:390–402.
- Burton A. S., Glavin D. P., Elsila J. E., Dworkin J. P., Jenniskens P., and Yin Q.-Z. 2014a. The amino acid composition of the Sutter’s Mill CM2 carbonaceous chondrite. *Meteoritics & Planetary Science* 49:2074–2086.
- Burton A. S., Grunsfeld S., Elsila J. E., Glavin D. P., and Dworkin J. P. 2014b. The effects of parent-body hydrothermal heating on amino acid abundances in CI-like chondrites. *Polar Science* 8:255–263.
- Burton A. S., McLain H., Glavin D. P., Elsila J. E., Davidson J., Miller K. E., Andronikov A. V., Lauretta D., and Dworkin J. P. 2015. Amino acid analyses of R and CK chondrites. *Meteoritics & Planetary Science* 50:470–482.
- Carré V., Aubriet F., and Muller J.-F. 2005. Analysis of cigarette smoke by laser desorption mass spectrometry. *Analytica Chimica Acta* 540:257–268.
- Chaumard N., Defouilloy C., and Kita N. T. 2018. Oxygen isotope systematics of chondrules in the Murchison CM2 chondrite and implications for the CO-CM relationships. *Geochimica et Cosmochimica Acta* 228:220–224.
- Clark B. E., Binzel R. P., Howell E. S., Cloutis E. A., Ockert-Bell M., Christensen P., Barucci M. A., DeMeo F., Lauretta D. S., Connolly H., Soderberg A., Hergenrother C., Lim L., Emery J., and Mueller M. 2011. Asteroid (101955) 1999 RQ<sub>36</sub>: Spectroscopy from 0.4 to 2.4 mm and meteorite analogs. *Icarus* 216:462–475.
- Clayton R. N. and Mayeda T. K. 1999. Oxygen isotope studies of carbonaceous chondrites. *Geochimica et Cosmochimica Acta* 63:2089–2104.
- Cloutis E. A., Hudson P., Hiroi T., and Mann P. 2011. Spectral reflectance properties of carbonaceous chondrites: 2. CM chondrites. *Icarus* 216:309–346.
- Cloutis E. A., Hudon P., Hiroi T., and Gaffey M. J. 2012. Spectral reflectance properties of carbonaceous chondrites 4: Aqueously altered and thermally metamorphosed meteorites. *Icarus* 220:586–617.

- DeMeo F. E., Binzel R. P., Slivan S. M., and Bus S. J. 2009. An extension of the bus asteroid taxonomy into the near-infrared. *Icarus* 202:160–180.
- Ebihara M. and Sekimoto S. 2019. Halogen contents in meteorites (1) Carbonaceous chondrites (abstract #2338). 50th Lunar and Planetary Science Conference. CD-ROM.
- Elsila J. E., Aponte J. C., Blackmond D. G., Burton A. S., Dworkin J. P., and Glavin D. P. 2016. Meteoritic amino acids: Diversity in compositions reflects parent body histories. *ACS Central Science* 2:370–379.
- Eugster O., Herzog G. F., Marti K., and Caffee M. W. 2006. Irradiation records, cosmic-ray exposure ages, and transfer times of meteorites. In *Meteorites and the early solar system II*, edited by Lauretta D. S. and McSween H. Y. Jr. Tucson, Arizona: University of Arizona Press. pp. 829–851.
- Friedrich J. M., Wang M.-S., and Lipshutz M. E. 2002. Comparison of the trace element composition of Tagish Lake with other primitive carbonaceous chondrites. *Meteoritics & Planetary Science* 37:677–686.
- Fujiya W., Sugiura N., Hotta H., Ichimura K., and Sano Y. 2012. Evidence for the late formation of hydrous asteroids from young meteoritic carbonates. *Nature Communications* 3:627–632.
- Gilmour I. and Pillinger C. 1992. Isotopic differences between PAH isomers in Murchison. *Meteoritics* 27:224–225.
- Glavin D. P., Dworkin J. P., Aubrey A., Botta O., Doty J. H., Martins Z., and Bada J. L. 2006. Amino acid analyses of Antarctic CM2 meteorites using liquid chromatography-time of flight-mass spectrometry. *Meteoritics & Planetary Science* 41:889–902.
- Glavin D. P., Callahan M. P., Dworkin J. P., and Elsila J. E. 2010. The effects of parent body processes on amino acids in carbonaceous chondrites. *Meteoritics & Planetary Science* 45:1948–1972.
- Göpel C., Birck J.-L., Galy A., Barrat J.-A., and Zanda B. 2015. Mn-Cr systematics in primitive meteorites: Insights from mineral-separation and partial dissolution. *Geochimica et Cosmochimica Acta* 156:1–24.
- Gounelle M., Engrand C., Alard O., Bland P. A., Zolensky M. E., Russell S. S., and Duprat J. 2005. Hydrogen isotopic composition of water from fossil micrometeorites in howardites. *Geochimica et Cosmochimica Acta* 69:3431–3443.
- Graf T., Baur H., and Signer P. 1990. A model for the production of cosmogenic nuclides in chondrites. *Geochimica et Cosmochimica Acta* 54:2521–2534.
- Guo W. and Eiler J. M. 2016. Temperatures of aqueous alteration and evidence for methane generation on the parent bodies of the CM chondrites. *Geochimica et Cosmochimica Acta* 71:5565–5575.
- Halliday I. and McIntosh B. A. 1990. Orbit of the Murchison meteorite. *Meteoritics & Planetary Science* 25:339–340.
- Hamilton V. E., Simon A. A., Christensen P. R., Reuter D. C., Clark B. E., Barucci M. A., Bowles N. E., Boynton W. V., Brucato J. R., Cloutis E. A., Connolly H. C., Donaldson Hanna K. L., Emery J. P., Enos H. L., Fornasier S., Haberle C. W., Hanna R. D., Howell E. S., Kaplan H. H., Keller L. P., Lantz C., Li J.-Y., Lim L. F., McCoy T. J., Merlin F., Nolan M. C., Praet A., Rozitis B., Sandford S. A., Schrader D. L., Thomas C. A., Zou X.-D., Lauretta D. S., and the OSIRIS-REx Team. 2019. Evidence for widespread hydrated minerals on asteroid (101955) Bennu. *Nature Astronomy* 3:332–340. doi:10.1038/s4155019-07222-2.
- Heis E. 1877. *Resultate der in den 43 Jahren 1833–1875 angestellten Sternschnuppen beobachtungen*. Königl. Sternwarte zu München, Verlag der M. DuMont-Schauber'schen Buchhandlung, Köln, pp. 141–142.
- Hewins R. H., Bourot-Denise M., Zanda B., Leroux H., Barrat J.-A., Humayun M., Göpel C., Greenwood R. C., Franchi I. A., Pont S., Lorand J.-P., Cournède C., Gattacceca J., Rochette P., Kuga M., Marroucchi Y., and Marty B. 2014. The Paris meteorite, the least altered CM chondrite so far. *Geochimica et Cosmochimica Acta* 124:190–222.
- Howard K. T., Alexander C. M. O'D., Schrader D. L., and Dyl K. A. 2015. Classification of hydrous meteorites (CR, CM and C2 ungrouped) by phyllosilicate fraction: PSD-XRD modal mineralogy and planetesimal environments. *Geochimica et Cosmochimica Acta* 149:206–222.
- Ishiguro M., Kuroda D., Hasegawa S., Kim M.-J., Choi Y.-J., Moskovitz N., Abe S., Pan K.-S., Takahashi J., Takagi Y., Arai A., Tokimasa N., Hsieh H. H., Thomas-Osip J. E., Osip D. J., Abe M., Yoshikawa M., Urakawa S., Hanyama H., Sekiguchi T., Wada K., Sumi T., Tristram P. J., Furusawa K., Abe F., Fukui A., Nagayama T., Warjurkar D. S., Rau A., Greiner J., Schady P., Knust F., Usui F., and Müller T. G. 2014. Optical properties of (162173) 1999 JU3: In preparation for the JAXA Hayabusa2 sample return mission. *Astrophysical Journal* 792:74–83.
- Jarosewich E. 1990. Chemical analysis of meteorites: A compilation of stony and iron meteorite analysis. *Meteoritics* 25:323–337.
- Jenniskens P. 2019. Review of asteroid-family and meteorite-type links. *Astronomy in Focus* 13. (in press).
- Jenniskens P., Fries M. D., Yin Q.-Z., Zolensky M., Kort A. N., Sandford S. A., Sears D., Beauford R., Ebel D. S., Friedrich J. M., Nagashima K., Wimpenny J., Yamakawa A., Nishiizumi K., Hamajima Y., Caffee M. W., Welten K. C., Laubenstein M., Davis A. M., Simon S. B., Heck P. R., Young E. D., Kohl I. E., Thiemens M. H., Nunn M. H., Mikouchi T., Hagiya K., Ohsumi K., Cahill T., Lawton J. A., Barnes D., Steele A., Rochette P., Verosub K., Gattacceca J., Cooper G., Glavin D. P., Burton A. S., Dworkin J. P., Elsila J., Pizzarello S., Oglione R., Schmitt-Kopplin P., Harir M., Hertkorn N., Verchovsky A., Grady M., Nagao K., Okazaki R., Takechi H., Hiroi T., Smith K., Silber E. A., Bronw P. G., Albers J., Klotz D., Hankey M., Matson R., Fries J. A., Walker R. J., Puchtel I., Lee C.-T. A., Erdman M. E., Epich G. R., Roeske S., Gabelica Z., Lerche M., Nuevo M., Girten B., and Worden S. P. 2012. Radar-enabled recovery of the Sutter's Mill meteorite, a carbonaceous chondrite regolith breccia. *Science* 338:1583–1587.
- Jenniskens P., Rubin A. E., Yin Q.-Z., Sears D. W. G., Sandford S. A., Zolensky M. E., Krot A. N., Blair L., Kane D., Utas J., Verish R., Friedrich J. M., Wimpenny J., Eppich G. R., Ziegler K., Verosub K. L., Rowland D. J., Albers J., Gural P. S., Grigsby B., Fries M. D., Matson R., Johnston M., Silber E., Brown P., Yamakawa A., Sanborn M. E., Laubenstein M., Welten K. C., Nishiizumi K., Meier M. M. M., Busemann H., Clay P., Caffee M. W., Schmitt-Kopplin P., Hertkorn N., Glavin D. P., Callahan M. P., Dworkin J. P., Wu Q., Zare R. N., Grady

- M., Verchovsky S., Emel'yanenko V., Naroenkov S., Clark D. L., Girten B., and Worden P. S. 2014. Fall, recovery and characterization of the Novato L6 chondrite breccia. *Meteoritics & Planetary Science* 49:1388–1425.
- Jenniskens P., Utas J., Yin Q.-Z., Matson R. D., Fries M., Howell J. A., Free D., Albers J., Devillepoix H., Bland P., Miller A., Verish R., Garvie L. A., Zolensky M. E., Ziegler K., Sanborn M. E., Verosub K. L., Rowland D. J., Ostrowski D. R., Bryson K., Laubenstein M., Zhou Q., Li Q.-L., Li X.-H., Liu Y., Tang G.-Q., Welten K., Meier M. M. M., Plant A. A., Maden C., Busemann H., and Granvik M. 2019. The Creston, California, meteorite fall and the origin of L chondrites. *Meteoritics & Planetary Science* 54:699–720. <https://doi.org/10.1111/maps.13235>
- Kimura M., Grossman J. N., and Weismberg M. K. 2011. Fe-Ni metal and sulfide minerals in CM chondrites: An indicator for thermal history. *Meteoritics & Planetary Science* 48:431–442.
- King A. J., Schofield P. F., and Russell S. S. 2017. Type 1 aqueous alteration in CM carbonaceous chondrites: Implications for the evolution of water-rich asteroids. *Meteoritics & Planetary Science* 52:1197–1215.
- King A. J., Greenwood R. C., Gibson J. M., Schofield P. F., Franchi I. A., and Russell S. S. 2018. The oxygen isotope composition of the most aqueously altered CM carbonaceous chondrites (abstract #2201). 49th Lunar and Planetary Science Conference. CD-ROM.
- Kitazato K., Milliken R. E., Iwata T., Abe M., Ohtake M., Matsuura S., Arai T., Nakauchi Y., Nakamura T., Matsuoka M., Seshu H., Hirata N., Hiroi T., Pilorget C., Brunetto R., Pouet F., Riu L., Bibring J.-P., Takir D., Domingue D. L., Filas F., Barucci M. A., Perna D., Palomba E., Galiano A., Tsumura K., Osawa T., Komatsu M., Nakato A., Arai T., Takato N., Matsunaga T., Takagi Y., Matsumoto K., Kouyama T., Yokota Y., Tatsumi E., Sakatani N., Yamamoto Y., Okada T., Sugita S., Honda R., Morota T., Kameda S., Sawada H., Honda C., Yamada M., Suzuki H., Yoshioka K., Hayakawa M., Ogawa K., Cho Y., Shirai K., Shimaki Y., Hirata N., Yamaguchi A., Ogawa N., Terui F., Yamaguchi T., Takei Y., Saiki T., Nakazawa S., Tanaka S., Yoshikawa M., Watanabe S., and Tsuda Y. 2019. The surface composition of asteroid 162173 Ryugu from Hayabusa2 near-infrared spectroscopy. *Science*. <https://doi.org/10.1126/science.aav7432>.
- Kollár D., Michel R., and Masarik J. 2006. Monte Carlo simulation of GCR neutron capture production of cosmogenic nuclides in stony meteorites and lunar surface. *Meteoritics & Planetary Science* 41:375–389.
- Kourtchev I., Godoi R. H. M., Connors S., Levine J. G., Archibald A. T., Godoi A. F. L., Paralovo S. L., Barbosa C. G. G., Souza R. A. F., Manzi A. O., Seco R., Sjøstedt S., Park J.-H., Guenther A., Kim S., Smith J., Martin S. T., and Kalberer M. 2016. Molecular composition of organic aerosols in central Amazonia: An ultra-high-resolution mass spectrometry study. *Atmospheric Chemistry & Physics* 16:11,899–11,913.
- Kurat G. and Kracher A. 1975. Preliminary report on the Cochabamba carbonaceous chondrite. *Meteoritics* 10:432–433.
- Langbroek M., De Kort N., Kriegsman L. M., Ziegler K., Zolensky M., and Van Westrenen W. 2015. Diepenveen (In A. Bouvier, J. Gattacceca, C. Agee, J. Grossman, K. Metzler 2017. The Meteoritical Bulletin, No. 104). *Meteoritics & Planetary Science* 52:23–24. <https://doi.org/10.1011/maps.12930>.
- Lantz C., Binzel R. P., and DeMeo F. E. 2018. Space weathering trends on carbonaceous asteroids: A possible explanation for Bennu's blue slope? *Icarus* 302:10–17.
- Lauretta D. S. 2015. OSIRIS-Rex Sample Return Mission. In *Handbook of cosmic hazards and planetary defense*, edited by Pelton J. N. and Allahdadi F. Berlin, Germany: Springer Verlag. pp. 543–567.
- Lazzaro D., Barucci M. A., Perna D., Jasmim F. L., Yoshikawa M., and Carvano J. M. F. 2013. Rotational spectra of (162173) 1999 JU3, the target of the Hayabusa2 mission. *Astronomy & Astrophysics* 549:L2–L4.
- Le Corre L., Sanchez J. A., Reddy V., Takir D., Cloutis E. A., Thirouin A., Becker K. J., Li J.-Y., Sugita S., and Tatsumi E. 2018. Ground-based characterization of Hayabusa2 mission target 162173 Ryugu: Constraining mineralogical composition in preparation for spacecraft operations. *Monthly Notices of the Royal Astronomical Society* 475:614–623.
- Lee M. R., Sofe M. R., and Lindgren P. 2014. Aragonite, breunnerite, calcite and dolomite in the CM carbonaceous chondrites: High fidelity recorders of progressive parent body aqueous alteration. *Geochimica et Cosmochimica Acta* 144:126–156.
- Lee M. R., Cohen B. E., Mark D. F., and Boyce A. 2018. Evidence for widespread post-hydration heating of the CM carbonaceous chondrites (abstract #1285). 49th Lunar and Planetary Science Conference. CD-ROM.
- Leya I. and Masarik J. 2009. Cosmogenic nuclides in stony meteorites revisited. *Meteoritics & Planetary Science* 44:1061–1086.
- Lindgren P., Lee M. R., Starkey N. A., and Franchi I. A. 2017. Fluid evolution in CM carbonaceous chondrites tracked through the oxygen isotopic compositions of carbonates. *Geochimica et Cosmochim. Acta* 204:240–251.
- Lingenfelter R. E., Canfield E. H., and Hess W. N. 1961. The lunar neutron flux. *Journal of Geophysical Research* 66:2665–2671.
- Lodders K. and Fegley B. 1998. *The planetary scientist's companion*. New York: Oxford University Press. 372 pp.
- Lodders K. 2003. Solar system abundances and condensation temperatures of the elements. *Astrophysical Journal* 591:1220–1247.
- Lunning N. G., Corrigan C. M., McSween H. Y., Tenner T. J., Kita N. T., and Bodnar R. J. 2016. CV and CM chondrite impact melts. *Geochimica et Cosmochimica Acta* 189:338–358.
- MacKinnon I. D. R. and Zolensky M. E. 1984. Proposed structures for poorly characterized phases in C2M carbonaceous chondrite matrix. *Nature* 309:240–242.
- MacPherson G. J. and Davis A. M. 1994. Refractory inclusions in the prototypical CM chondrite, Mighei. *Geochimica et Cosmochimica Acta* 58:5599–5625.
- Martins Z., Modica P., Zanda B., and D'Hendecourt L. L.-S. 2015. The amino acid and hydrocarbon contents of the Paris meteorite: Insights into the most primitive CM chondrite. *Meteoritics & Planetary Science* 50:926–943.
- Masarik J. and Reedy R. C. 1994. Effects of bulk composition on nuclide production processes in meteorites. *Geochimica et Cosmochimica Acta* 58:5307–5317.

- Meier M. M. M., Schmitz B., Alwmark C., Trappitsch R., Maden C., and Wieler R. 2014. He and Ne in individual chromite grains from the regolith breccia Ghubara (L5): Exploring the history of the L chondrite parent body regolith. *Meteoritics & Planetary Science* 49:576–594.
- Meier M. M. M., Grimm S., Maden C., and Busemann H. 2016. Do we have meteorites from the Veritas asteroid break-up event 8 Ma ago? (abstract #6291). 79th Annual meeting of the Meteoritical Society.
- Michel P., Jutzi M., Richardson D. C., and Benz W. 2010. The asteroid Veritas: An intruder in a family named after it? *Icarus* 211:535–545.
- Müller T. G., Durech J., Hasegawa S., Abe M., Kawakami K., Kasuga T., Kinoshita D., Kuroda D., Urakawa S., Okumura S., Sarugaku Y., Miyasaka S., Takagi Y., Weissman P. R., Choi Y.-J., Larson S., Yanagisawa K., and Nagayama S. 2011. Thermo-physical properties of 162173 (1999 JU3), a potential flyby and rendezvous target for interplanetary missions. *Astronomy & Astrophysics* 525:A145–A151.
- Munsell A. H. 1954. *Munsell soil color charts*. Baltimore, Maryland: Munsell Color Company Inc. 10 p.
- Nakamura T. 2006. Yamato 793321 CM chondrite: Dehydrated regolith material of a hydrous asteroid. *Earth & Planetary Science Letters* 242:26–38.
- Nakamura T., Nagao K., Metzler K., and Takaoka N. 1999. Heterogeneous distribution of solar and cosmogenic noble gases in CM chondrites and implications for the formation of CM parent bodies. *Geochimica et Cosmochimica Acta* 63:257–273.
- Nazarov M. A., Brandstaetter F., and Kurat G. 1996. Phosphides and P-rich sulfides in the Mighei (CM) chondrite. *Lunar and Planetary Science Conference* 27:939–940.
- Nesvornyy D., Bottke W. F., Levison H. F., and Dones L. 2003. Recent origin of the solar system dust bands. *Astrophysical Journal* 591:486–497.
- Nishiizumi K. 2004. Preparation of  $^{26}\text{Al}$  AMS standards. *Nuclear Instruments and Methods in Physics Research* B223–224:388–392.
- Nishiizumi K. and Caffee M. W. 2012. Exposure histories of C11 and CM2 carbonaceous chondrites (abstract #2758). 48th Lunar and Planetary Science Conference. CD ROM.
- Nishiizumi K., Imamura M., Caffee M. W., Southon J. R., Finkel R. C., and McAninch J. 2007. Absolute calibration of  $^{10}\text{Be}$  AMS standards. *Nuclear Instruments and Methods in Physics Research* B258:403–413.
- Oba Y. and Naraoka H. 2009. Elemental and isotope behavior of macromolecular organic matter from CM chondrites during hydrous pyrolysis. *Meteoritics & Planetary Science* 44:943–953.
- Ott U. 2014. Planetary and pre-solar noble gases in meteorites. *Chemie der Erde — Geochemistry* 74:519–544.
- Pearson V. K., Sephton M. A., Franchi I. A., Gibson J. M., and Gilmour I. 2006. Carbon and nitrogen in carbonaceous chondrites: Elemental abundances and stable isotopic compositions. *Meteoritics & Planetary Science* 41:1899–1918.
- Perna D., Barucci M. A., Ishiguro M., Alvarez-Candal A., Kuroda D., Yoshikawa M., Kim M.-J., Fornasier S., Hasegawa S., Roh D.-G., Müller T. G., and Kim Y. 2017. Spectral and rotational properties of near-Earth asteroid (162173) Ryugu, target of the Hayabusa2 sample return mission. *Astronomy & Astrophysics* 599: L1–L4.
- Piani L., Yurimoto H., and Remusat L. 2018. A dual origin for water in carbonaceous asteroids revealed by CM chondrites. *Nature Astronomy* 2:317–323.
- Pignatelli I., Marrocchi Y., Mugnaioli E., Bourdelle F., and Gounelle M. 2017. Mineralogical, crystallographic and redox features of the earliest stages of fluid alteration in CM chondrites. *Geochimica et Cosmochimica Acta* 209:106–122.
- Popova O. P., Jenniskens P., Emel'yanenko V., Kartashova A., Biryukov E., Khaibrakhmanov S., Shuvalov V., Rybnov Y., Dudorov A., Grokhovsky V. I., Badyukov D. D., Yin Q.-Z., Gural P. S., Albers J., Granvik M., Evers L. G., Kuiper J., Kharlamov V., Solovyov A., Rusakov Y. S., Korotkiy S., Serdyuk I., Korochantsev A. V., Larionov M. Y., Glazachev D., Mayer A. E., Gisler G., Gladkovsky S. V., Wimpenny J., Sanborn M. E., Yamakawa A., Verosub K., Rowland D. J., Roeske S., Botto N. W., Friedrich J. M., Zolensky M., Le L., Ross D., Ziegler K., Nakamura T., Ahn I., Lee J. I., Zhou Q., Li X.-H., Li Q.-L., Liu Y., Tang G.-Q., Hiroi T., Sears D., Weinstein I. A., Vokhmintsev A. S., Ishchenko A. V., Schmitt-Kopplin P., Hertkorn N., Nagao K., Haba M. K., Komatsu M., and Mikouchi T. 2013. Chelyabinsk airburst, damage assessment, meteorite recovery, and characterization. *Science* 342:1069–1073.
- Ray D. and Shukla A. D. 2018. The Mukundpura meteorite, a new fall of CM chondrite. *Planetary and Space Science* 151:149–154.
- Rodgman A. and Perfetti T. A. 2006. The composition of cigarette smoke: A catalogue of the polycyclic aromatic hydrocarbons. *Beiträge zur Tabakforschung International/Contributions to Tobacco Research* 22:13–69.
- Rubin A. E. 2012. Collisional facilitation of aqueous alteration in CM and CV carbonaceous chondrites. *Geochimica et Cosmochimica Acta* 90:181–194.
- Rubin A. E. 2015. An American on Paris: Extent of aqueous alteration of a CM chondrite and the petrography of its refractory and amoeboid olivine inclusions. *Meteoritics & Planetary Science* 50:1595–1612.
- Rubin A. E., Trigo-Rodríguez J. M., Huber H., and Wasson J. T. 2007. Progressive aqueous alteration of CM carbonaceous chondrites. *Geochimica et Cosmochimica Acta* 71:2361–2382.
- Ruf A., Kanawati B., Hertkorn N., Yin Q.-Z., Moritz F., Harir M., Lucio M., Michalke B., Wimpenny J., Shilobreeva S., Bronsky B., Saraykin V., Gabelica Z., Gougeon R., Quirico E., Ralew S., Jakubossi T., Haack H., Gonsior M., Jenniskens P., Hinman N. W., and Schmitt-Kopplin P. 2017. Previously unknown class of metalorganic compounds revealed in meteorites. *Proceedings of the National Academy of Sciences* 114:2819–2824.
- Rumble D., Miller M. F., Franchi I. A., and Greenwood R. C. 2007. Oxygen three-isotope fractionation lines in terrestrial silicate minerals: An inter-laboratory comparison of hydrothermal quartz and eclogite garnet. *Geochimica et Cosmochimica Acta* 71:3592–3600.
- Schmitt-Kopplin P., Gabelica Z., Gougeon R. D., Fekete A., Kanawati B., Harir M., Gebefuegi I., Eckel G., and Hertkorn N. 2010. High molecular diversity of extraterrestrial organic matter in Murchison meteorite

- revealed 40 years after its fall. *Proceedings of the National Academy of Sciences* 107:2763–2768.
- Sharma P., Kubik P. W., Fehn U., Gove G. E., Nishiizumi K., and Elmore D. 1990. Development of  $^{36}\text{Cl}$  standards for AMS. *Nuclear Instruments and Methods in Physics Research* B52:410–415.
- Sharma P., Bourgeois M., Elmore D., Granger D., Lipschutz M. E., Ma X., Miller T., Mueller K., Rickey F., Simms P., and Vogt S. 2000. PRIME lab AMS performance, upgrades and research applications. *Nuclear Instruments and Methods in Physics Research* B172:112–123.
- Shields W. R., Murphy T. J., Catanzaro E. J., and Garner E. L. 1966. Absolute isotopic abundance ratios and the atomic weight of a reference sample of chromium. *Journal of Research of the National Bureau of Standards* 70A:193–197.
- Tonui E., Zolensky M., Hiroi T., Nakamura T., Lipschutz M. E., Wang M.-S., and Okudaira K. 2014. Petrographic, chemical and spectroscopic evidence for thermal metamorphism in carbonaceous chondrites. *Geochimica et Cosmochimica Acta* 126:284–306.
- Trigo-Rodriguez J. M., Rubin A. E., and Wasson J. T. 2006. Non-nebular origin of dark mantles around chondrules and inclusions in CM chondrites. *Geochimica et Cosmochimica Acta* 70:1271–1290.
- Turrin B., Lindsay F. N., Park J., Herzog G. F., Delaney J. S., and Swisher C. C. 2014.  $^{40}\text{Ar}/^{39}\text{Ar}$  studies of Murchison (CM2) and Tagish Lake (2-ung) (abstract #2485). 45th Lunar and Planetary Science Conference. CD-ROM.
- Tziotis D., Hertkorn N., and Schmitt-Kopplin P. 2011. Kendrick-analogous network visualisation of ion cyclotron resonance Fourier transform (FTICR) mass spectra: Improved options to assign elemental compositions and to classify organic molecular complexity. *European Journal of Mass Spectrometry* 17:415–421.
- Unsalan O., Jenniskens P., Yin Q.-Z., Kyagisiz E., Albers J., Clark D. L., Granvik M., Demirkol I., Erdogan I. Y., Bengu A. S., Ozel M. E., Terzioglu Z., Gi N., Brown P., Yalcinkaya E., Temel T., Prabhu D. K., Robertson D. K., Boslough M., Ostrowski D. R., Kimberley J., Er S., Rowland D. J., Bryson K. L., Altunayar-Unsalan C., Rangelov B., Karamanov A., Tatchev D., Kocahan O., Oshtrakh M. I., Maksimova A. A., Karabanalov M. S., Verosub K. L., Levin E., Yusal I., Hoffmann V., Hiroi T., Reddy V., Ildiz G. O., Bolukbasi O., Zolensky M. E., Hochleitner R., Kaliwoda M., Ongen S., Fausto R., Nogueira B. A., Chukin A. V., Karashanova D., Semionkin V. A., Yesiltas M., Glotch T., Yilmaz A., Friedrich J. M., Sanborn M. E., Huyskens M., Ziegler K., Williams C. D., Schonbachler M., Bauer K., Meier M. M. M., Maden C., Busemann H., Welten K. C., Caffee M. W., Laubenstein M., Zhou Q., Li Q.-L., Li X.-H., Tang G.-Q., Sears D. W. G., McLain H. L., Dworkin J. P., Elsila J. E., Glavin D. P., Schmitt-Kopplin P., Ruf A., Le Corre L., Schmedemann N., and The Saricicek meteorite consortium. 2019. The saricicek howardite fall in Turkey: Source crater of HED meteorites on Vesta and impact risk of Vestoids. *Meteoritics & Planetary Science*. <https://doi.org/10.1111/maps.13258>.
- Ushikubo T., Kimura M., Kita N. T., and Valley J. W. 2012. Primordial oxygen isotope reservoirs of the solar nebula recorded in chondrules in Acfer 094 carbonaceous chondrite. *Geochimica et Cosmochimica Acta* 90:242–264.
- Vacher L., Marrocchi Y., Villeneuve J., Verdier-Paoletti M., and Gounelle M. 2017. Petrographic and C&O isotopic characteristics of the earliest stages of aqueous alteration of CM chondrites. *Geochimica et Cosmochimica Acta* 213:271–290.
- Verdier-Paoletti M., Marrocchi Y., Avice G., and Gounelle M. 2017. Oxygen isotope constraints on the alteration temperatures of CM chondrites. *Earth and Planetary Science Letters* 458:273–281.
- Vilas F. 2008. Spectral characteristics of Hayabusa2 Near-Earth asteroid targets 1999 JU3 and 2001 QC34. *The Astronomical Journal* 135:1101–1105.
- Vinogradoff V., Le Guillou C., Bernard S., Binet L., Cartigny P., Brearley A. J., and Remusat L. 2017. Paris vs. Murchison: Impact of hydrothermal alteration on organic matter in CM chondrites. *Geochimica et Cosmochimica Acta* 212:234–252.
- Walker G. J. 1874. Fireball. *Astronomical Register* 12:17.
- Wang J., Hu Y., Xu Y., Tian Z., and Pan Y. 2017. On-line photoionization mass spectrometric study on the mouth retention of gaseous mainstream cigarette smoke. *Analytical Methods* 9:3643–3652.
- Wasson J. T. and Kallemeyn G. W. 1988. Compositions of Chondrites. *Philosophical Transactions of the Royal Society of London. Series A, Mathematical and Physical Sciences* 325:535–544.
- Wetherill G. 1985. Asteroidal source of ordinary chondrites. *Meteoritics* 20:1–22.
- Wieler R., Baur H., Pedroni A., Signer P., and Pellas P. 1989. Exposure history of the regolithic chondrite Fayetteville: I. Solar-gas-rich matrix. *Geochimica et Cosmochimica Acta* 53:1441–1448.
- Wu Q., Pomerantz A. E., Mullins O. C., and Zare R. N. 2013. Minimization of fragmentation and aggregation by laser desorption laser ionization mass spectrometry. *Journal of the American Society for Mass Spectrometry* 24:1116–1122.
- Yamakawa A., Katsuyuki Y., Makishima A., and Nakamura E. 2009. Chemical separation and mass spectrometry of Cr, Fe, Ni, Zn, and Cu in terrestrial and extraterrestrial materials using thermal ionization mass spectrometry. *Analytical Chemistry* 81:9787–9794.
- Yanai K., Kojima H., and Haramura H. 1995. Chemical compositions of the Antarctic meteorites. In *Catalog of the Antarctic meteorites*, edited by Hirasawa T. Tokyo, Japan: National Institute of Polar Research. pp. 44–76.
- Yassine M., Harir M., Dabek-Zlotorzynska E., and Schmitt-Kopplin P. 2014. Structural characterization of organic aerosol using Fourier transform ion cyclotron resonance mass spectrometry. Aromaticity equivalent approach. *Rapid Communications in Mass Spectrometry* 28:2445–2454.
- Yin Q.-Z., Yamashita K., Yamakawa A., Tanaka R., Jacobsen B., Ebel D., Hutcheon I. D., and Nakamura E. 2009.  $^{55}\text{Mn}$ - $^{53}\text{Cr}$  systematics of Allende chondrules and  $\epsilon^{54}\text{Cr}$ - $\Delta^{17}\text{O}$  correlation in bulk carbonaceous chondrites (abstract #2006). 40th Lunar and Planetary Science Conference. CD-ROM.
- Young E. D. 2001. The hydrology of carbonaceous chondrite parent bodies and the evolution of planet progenitors. *Philosophical Transactions of the Royal Society. A. Mathematical, Physical and Engineering Sciences* 359:2095–2110.
- Young E. D. and Russell S. S. 1998. Oxygen reservoirs in the early solar nebula inferred from an Allende CAI. *Science* 282:452–455.

- Zolensky M. E., Bourcier W. L., and Gooding J. L. 1989. Aqueous alteration on the hydrous asteroids—Results of computer simulations. *Icarus* 78:411–425.
- Zolensky M. E., Barrett R. A., and Browning L. 1993. Mineralogy and composition of matrix and chondrule rims in carbonaceous chondrites. *Geochimica et Cosmochimica Acta* 57:3123–3148.
- Zolensky M. E., Mittlefehldt D. W., Lipschutz M. E., Wang M.-S., Clayton R. N., Mayeda T., Grady M. M., Pillinger C., and Barber D. 1997. CM chondrites exhibit the complete petrologic range from type 2 to 1. *Geochimica et Cosmochimica Acta* 61:5099–5115.
- Zolensky M., Mikouchi T., Hagiya K., Ohsumi K., Komatsu M., and Le L. 2015. Evidence for impact shock melting in CM and CI chondrite regolith samples (abstract #2261). 46th Lunar and Planetary Science Conference. CD-ROM.
-